HIGH MECHANICS AND AUTOMOTIVE DESIGN AND TECHNOLOGY

XXV Doctorate Cycle

UNIVERSITY OF MODENA AND REGGIO EMILIA

Department of Engineering Enzo Ferrari

A Linear Complementarity Approach to Solve Elastohydrodynamic Lubrication Problems in the Presence of Cavitation

Candidate:

Luca Bertocchi

Supervisor:

Prof. Antonio Strozzi

March 2013

Thesis submitted for the Degree of Doctor of Philosophy

School Director/Coordinator: Prof. Paolo Tartarini

Declaration of Authorship

I, Luca Bertocchi, declare that this thesis titled, 'A Linear Complementarity Approach to Solve Elastohydrodynamic Lubrication Problems in the Presence of Cavitation' and the work presented in it are my own. I confirm that:

- This work was done wholly or mainly while in candidature for a research degree at this University.
- Where any part of this thesis has previously been submitted for a degree or any other qualification at this University or any other institution, this has been clearly stated.
- Where I have consulted the published work of others, this is always clearly attributed.
- Where I have quoted from the work of others, the source is always given. With the exception of such quotations, this thesis is entirely my own work.
- I have acknowledged all main sources of help.
- Where the thesis is based on work done by myself jointly with others, I have made clear exactly what was done by others and what I have contributed myself.

Signed: _____

Date: _____

"Who wrote this PhD Thesis?"

Me

UNIVERSITY OF MODENA AND REGGIO EMILIA

Abstract

Department of Engineering Enzo Ferrari

Doctor of Philosophy

by Luca Bertocchi

This formulation is based on the Reynolds equation, appropriately recasted in terms of pressure and void fraction. The correct detection of the cavitation and the location of the boundaries between cavitated and active areas is guaranteed by the complementary nature of the two chosen variables. Therefore, it is possible to describe the hydrodynamic problem all over the domain using a single equation, which is valid both in the active and in the cavitated zone. This approach naturally guarantees the mass conservation. A detailed analysis of the proposed complementary formulation of the Reynolds equation is presented, both for one dimensional and two dimensional cases. In addition, various rheological models are considered in order to simulate accurately the lubricant behaviour and properties. The Hertz contact theory has been introduced for the consideration of the elastic deflection of the contact bodies. As an alternative, it is possible to handle the elasticity of the solids by importing the compliance matrix generated by a external structural Finite Element model. This second method is suitable for the EHL analysis of various common mechanical components, such connecting rods big end and small end bearings, that cannot be satisfactorily modelled with the Hertz contact theory. A numerical method, based on the Finite Element framework, has been employed to solve the complementarity formulation of the Reynolds equation. The developed implementation is versatile and robust and does not require particular conditions on the dimensions of the elements of the mesh. The numerical development focused on the maximization of the computational speed. The proposed formulation is capable to solve efficiently a wide range of problems and to consider various rheological and elastic models. Particular advantages, with respect to standard finite difference approaches, have been found in the cases of isoviscous and rigid lubrication regimes and in the presence of steep film thickness gradients.

Acknowledgements

My gratitude goes to my supervisor Prof.Antonio Strozzi and to the three researcher of the Machine Design Group. To Ing.Matteo Giacopini, who introduced me to the magical world of Lubrication, who supported and leaded me in the development of my work. To Ing.Andrea Baldini, who works relentlessly to make the world a better place for PhD Students and, finally, to Ing.Enrico Bertocchi, for his genial ideas and the help he gives when all other hopes are lost.

Special thanks to all the people, past and present, of the Machine Design Group: Sara, Simone, Giuseppe, Luca - L, Luca - DAg, Alberto, Alessandro, Beppe, Eleonora, Dario, Enrico, Omer.

Many thanks go to Daniele Dini, for his precious support, for his help and guidance and for the possibility he and Matteo gave me to spend six months at the Tribology Group of the Imperial College.

I would like to thank all the people of the tribology lab of the Imperial College for their friendship and for the great time I had in London: Ioannis, Anant, Pavel, Johan, Antonio, Mark, Alex, Tom, Kazuhide, Jonathan, Jason. A very special thanks to Mario, Luca and Fabio, for all the time we spent together, for the launches, the coffees and all the workouts at the gym.

After all those long years of studies, I would like to thanks my parents (and brothers and sister), for the support, patience and help they gave me!

And, finally, a thanks to Veronica (who painted our future home and prepared all the invitations for our wedding while I was writing this thesis) for her love...

Have I forgotten someone? Please, don't blame me. It's four o'clock in the morning and the thesis submission it's tomorrom morning. In the case I have forgotten you, I will offer you a drink...

Contents

Declaration of Authorship iii

Abstract vii

Acknowledgements ix

List of Figures xv

Symbols xix

1 Introduction 1
1.1 Thesis Layout . . . 3

2 Complementarity Formulation 5
2.1 Governing Equations . . . 5
2.1.1 Reynolds Equation . . . 5
2.1.2 Compressibility . . . 6
Constant bulk modulus . . . 6
Dowson and Higginson model . . . 7
Jacobson and Vinet model . . . 7
2.1.3 Piezoviscosity . . . 8
Barus model . . . 8
Roelands model . . . 8
Doolittle's free-volume . . . 9
Rodermund . . . 9
2.1.4 Non-Newtonian Fluids . . . 9
Ree-Eyring . . . 10
Polynomial Shear Thinning Law . . . 10
2.2 Complementarity Formulation of the Reynolds Equation for Non-Linear Fluids . . . 10
2.2.1 Functional connection between the complementarity variables . . . 14
2.3 Numerical Implementation . . . 15

3 Elastic Deflection 21
3.1 Governing Equations . . . 21
3.1.1 Elastic Deflection . . . 22

3.1.1.1 Hertzian theory . . . 22
3.1.1.2 Finite Element contact model . . . 23
3.2 Numerical Implementation . . . 25
3.2.1 Newton method for EHL problems . . . 26
3.2.2 Finite Element discretization of the EHL Reynolds equation . . . 29

4 Numerical Implementation 33
4.1 Test Cases . . . 33
4.1.1 Parabolic Slider . . . 33
4.1.2 Journal bearing with piezoviscous lubricant . . . 36
4.1.3 Pure Squeeze . . . 38
4.1.4 2D Pocket . . . 39
4.2 Journal Bearing . . . 43
4.2.1 Governing Equations . . . 43
Reynolds equation for elastohydrodynamic lubrication . . . 43
Equilibrium equation . . . 44
Oil supply hole . . . 44
Lubricant model . . . 45
Elastic deflection . . . 45
4.2.2 Numerical Algorithm . . . 46
4.2.3 Results and Discussion . . . 48

5 Further Applications of the Concept of Complementarity to Lubrication 63
5.1 Slip at The Wall . . . 63
5.1.1 Complementarity Formulation for the Tangential Velocity Slip Problem . . . 64
5.1.2 Complementarity Formulation For the Slip at the Wall Problem in the Presence of Cavitation . . . 66
5.2 Mixed Lubrication . . . 67
5.2.1 Complementarity Formulation for Dry Contact Problems . . . 67
5.2.2 EHL Formulation for Mixed Lubrication in the Presence of Cavitation . . . 68

6 Conclusions and Future Development 71
6.1 Conclusions . . . 71
6.2 Future Development . . . 71

A Analytical model for two dimensional pure squeeze motion 73
A.1 Analytical model for two dimensional pure squeeze motion . . . 73

B Publications by the Author 77
B.1 Publications on the Topic . . . 77
B.2 Other Publications . . . 77

Bibliography **79**

List of Figures

2.1 a) Comparison of the solutions of the problem in 4.1.1 in terms of p and r using different integration points ξ_{int} and different upwind parameter α for the terms of Eqn.(2.46) and b) detail of the different solutions for r in the cavitated region 20

3.1 The two contribution to the total film thickness 21
3.2 Schematic of two contact bodies. The red nodes are contact (boundary) nodes while the blue ones are interior nodes 24

4.1 Schematic of the problem along with the description of the main symbol adopted 34
4.2 Pressure distribution for the different formulations considered 34
4.3 Comparison of the solutions obtained with different formulation for a single parabolic slider 34
4.4 Schematic of a twin parabolic slider 35
4.5 Pressure solutions for the different formulations considered 35
4.6 Comparison of the solutions obtained with different formulation for a single parabolic slider 35
4.7 Comparison of the pressure solutions for isoviscous (dashed lines) and piezoviscous (solid lines) lubricants for a statically loaded journal for an eccentricity ratio $e/c = 0.93$ 37
4.8 Comparison of the pressure solutions for isoviscous (dashed lines) and piezoviscous (solid lines) lubricants for a statically loaded journal for an eccentricity ratio $e/c = 0.95$ 37
4.9 Extension of the cavitated zone in a pure squeeze motion for the proposed formulation and for the analytical solution. 38
4.10 Schematic of a converging bearing containing a single micro-texture pocket, positioned toward the inlet, along with the description of the main symbol adopted (section π and isometric view) 40
4.11 Waffle slipper-like pressure profile 41
4.12 Normalized density 41
4.13 Pressure and normalized density for the two dimensional micro-texture pocket (i). The pocket width is $w = 7\,mm$. 41
4.14 Comparison of the pressure profiles in the mid-section π. The complementarity solution for the pocket $10\,mm$ wide is compared with the JFO formulation provided in [1], and the complementarity solution for the pocket $300\,mm$ wide is compared with the one dimensional solution. . . . 42
4.15 Schematic of the connecting rod assembly along with the most important dimensions, angles, geometrical and mass property 45

4.16 Crankshaft section. The position of the oil supply hole is highlighted and the meaning of the main symbols are depicted . . . 46
4.17 Mesh of the connecting rod . . . 46
4.18 External load for the connecting-rod bearing . . . 50
4.19 Load diagram for a connecting-rod bearing . . . 51
4.20 Comparison of the orbit diagrams for the journal bearing with and without the oil supply hole. Solid surfaces are elastic and the lubricant is compressible, piezoviscous and shear thinning. . . . 52
4.21 Minimum film thickness for the three cases analysed. . . . 53
4.22 Instant total mass of oil present in the lubricant film with and without the oil supply hole. . . . 54
4.23 Oil mass variation and total flow rate across the side boundary for the configuration without supply hole. . . . 54
4.24 Oil mass variation, oil flow rate across the boundaries for the configuration with the oil supply hole. . . . 55
4.25 Mass flux across the side boundary length during a complete engine cycle for the configuration without the oil supply hole. . . . 55
4.26 Mass flux across the side boundary length during a complete engine cycle for the configuration with the oil supply hole . . . 56
4.27 Hydrodynamic pressure . . . 57
4.28 Dry contact pressure . . . 57
4.29 Total pressure . . . 57
4.30 Void fraction . . . 57
4.31 Various plot regarding the EHL journal bearing analysis in the presence of the oil supply hole at a crank angle $\theta = 0$, which corresponds to the Top Dead Centre at the beginning of the power stroke. Note that no dry contact is detected. . . . 57
4.32 Hydrodynamic pressure . . . 58
4.33 Dry contact pressure . . . 58
4.34 Total pressure . . . 58
4.35 Void fraction . . . 58
4.36 Various plot regarding the EHL journal bearing analysis in the presence of the oil supply hole at a crank angle $\theta = 180$, which corresponds to the Bottom Dead Centre at the end of the power stroke. . . . 58
4.37 Hydrodynamic pressure . . . 59
4.38 Dry contact pressure . . . 59
4.39 Total pressure . . . 59
4.40 Void fraction . . . 59
4.41 Various plot regarding the EHL journal bearing analysis in the presence of the oil supply hole at a crank angle $\theta = 360$, which corresponds to the Top Dead Centre at the beginning of the intake stroke . . . 59
4.42 Hydrodynamic pressure . . . 60
4.43 Dry contact pressure . . . 60
4.44 Total pressure . . . 60
4.45 Void fraction . . . 60
4.46 Various plot regarding the EHL journal bearing analysis in the presence of the oil supply hole at a crank angle $\theta = 540$, which corresponds to the Bottom Dead Centre at the beginning of the compression stroke . . . 60

4.47 Crank angle $\theta = 0$ 61
4.48 Crank angle $\theta = 180$ 61
4.49 Crank angle $\theta = 360$ 61
4.50 Crank angle $\theta = 540$ 61
4.51 Film thickness distribution at different crank angle 61

5.1 Meaning of symbols τ and U^+ and the the shear stress sign convention for the tangential velocity slip problem 64

Symbols

$\Delta\Omega$	Determinant of the coordinate transformation	m
α	Upwind parameter	-
α_p	Pressure viscosity index	$(Pa)^{-1}$
β	Bulk modulus	Pa
$\dot{\gamma}$	Shear rate	$1/s$
$\eta_\prime$	Jacobson and Vinet coefficient	-
η	Local y coordinate	m
μ	Viscosity	Pas
μ_0	Base viscosity	Pas
μ_{Barus}	Barus viscosity	Pas
$\mu_{Roelands}$	Roelands viscosity	Pas
$\mu_{Doolittle}$	Doolittle viscosity	Pas
μ_{Eyring}	Eyring viscosity	Pas
$\mu_{Rodermund}$	Rodermund viscosity	Pas
ν	Poisson Ratio	-
ξ	Local x coordinate	m
ρ	Density	kg/m^3
ρ_c	Density at cavitation pressure	kg/m^3
ρ_p	Density of the liquid fraction	kg/m^3
τ_0	Eyring stress	Pa
θ_s	Supply hole angle	deg
ω	Rotating speed	rad/s
a	Domain length	m
a_r	Rodermund coefficient	Pa^{-1}
b	Domain width	m
b_r	Rodermund coefficient	-
B_0	Jacobson and Vinet coefficient	Pa
C	Compliance matrix	m/Pa

C_1	Dowson and Higginson coefficient	Pa
C_2	Dowson and Higginson coefficient	-
E	Young's Modulus	Pa
E_r	Reduced Young's Modulus	Pa
F_x	External force in x direction	N
F_y	External force in y direction	N
K	Stiffness matrix	N/m
K_0	Doolittle coefficient	Pa
K_0'	Doolittle coefficient	-
N	Shape function	-
U	Velocity	m/s
V_0	Doolittle coefficient	m^3
V_{occ}	Doolittle coefficient	m^3
W	Test function	-
Z	Roelands coefficient	-
c	Radial clearance	m
dt	Time step	s
e	Bearing eccentricity	m
$f(p)$	Compressibility factor	-
h	Film thickness	m
h_e	Elastic deflection	m
h_g	Undeformed film thickness	m
h_min	Minimum film thickness	m
h_max	Maximum film thickness	m
h_p	Pocket depth	m
l_cr	Connecting rod length	m
p	Pressure	Pa
p_{amb}	Ambient pressure	Pa
p_c	Cavitation pressure	Pa
p_{supply}	Supply tank pressure	Pa
p_s	Pressure at step s	Pa
r	Void fraction	-
r_c	Crank radius	mm
r_j	Journal radius	mm
t	Time	s
w	Gauss weight	-
x	Spatial coordinate along the direction of flow	m
y	Spatial coordinate perpendicular to x and film-thickness h	m
z	Spatial coordinate along the film thickness	m

Chapter 1

Introduction

"O studianti, studiate le matematiche, e non edificate sanza fondamenti"

Leonardo da Vinci

Reynolds equation is commonly used to describe lubrication problems as an alternative to the more complex full Navier-Stokes equation. The assumptions the Reynolds equation is based on are fully satisfied in the analysis of the majority of the lubricated bearing commonly found in practical applications. These assumptions are, namely, that both the ratio of the film thickness to the contact length and the Reynolds number are small.

Cavitation may occur due to the development of low pressures within the fluid film. Various formulations have been proposed in order to correctly simulate this phenomenon. In the cavitated regions the mechanical properties of the fluid vary significantly. Jakobsson and Floberg [2] proposed a mass conserving algorithm capable to analyse lubricant films in the presence of cavitation. The algorithm described in [2] uses ad-hoc equations to locate the cavitation boundaries, setting a fixed pressure value in the non-active regions while solving the Reynolds equation within the active counterparts. Elrod and Adams [3] first developed a cavitation algorithm that uses a single equation within the whole domain and does not require the explicit location of the cavitation boundaries. They introduced a switch function, $g(p)$, that equals one where the pressure is greater than the cavitation pressure (active zone) and it is null ($g(p) = 0$) otherwise (non active zone). In this way the Poiseuille term of the Reynolds equation can be artificially suppressed in the cavitated regiond. Starting from the pioneering works of Elrod [3, 4], further algorithms have been developed that took into account the compressibility of the lubricant, e.g. Vijayaraghavan and Keith [5] and Sahlin et al. [6].

Attempts have been made in the past to solve the problem of determining the active and cavitated film regions using the concept of complementarity [7–9]. However, these

classical methods based on a complementarity formulation do not ensure the conservation of mass. This undesired characteristic is due to the fact that such algorithms solve the Reynolds equation within the whole domain assuming a constant lubricant density. While this assumption can be reasonably accepted within the active regions, in the non-active regions density varies in both space and time. Giacopini et al. [10] explained how assuming constant fluid density within the whole domain leads to an incomplete identification of film rupture and, thus, to an incorrect detection of film reformation. Therefore, ensuring the mass continuity is mandatory to correctly predict the film rupture and reformation, especially where cavitation and reformation occur several times (e.g. studies of rough contacts [11], textured surfaces [1, 12, 13] and dynamically loaded journal bearings [14]). The algorithm proposed in [10] ensures the conservation of mass within the whole domain, employing a complementarity formulation of the lubrication problem in the presence of cavitation based on a newly defined set of complementarity variables.

The work presented in [10] deals with incompressible and isoviscous fluids, thus providing good results only for low contact pressures, where the density and viscosity variations in the active regions are negligible. However, the increasing quest for enhanced performance, the severity of operating conditions to which bearings can be subjected, and a constant need for more accurate predictions, has been responsible for the development of new formulations that take into account several lubricant behaviours not compatible with the classical Reynolds equation. In particular, at high pressures the compressibility of the fluid, the piezoviscosity and non-Newtonian behaviour can no longer be neglected. Therefore, new formulations have been proposed, that overcome the limitations that the hypothesis of incompressibility and isoviscosity introduced in the classical formulations. Although various authors in recent years studied the lubricant film behaviour employing the full Navier-Stokes equations in CFD solvers [15, 16], Reynolds-based approaches maintain great importance and practical utility due to their simpler formulations, that lead to usually faster and less CPU-time consuming implementations and provide equal accuracy for all the (many) scenarios in which the change in fluid properties through film-thickness are negligible.

In the present work, the formulation of the Reynolds equation in terms of complementarity is first extended to handle compressible, piezoviscous and shear-thinning fluids. Then, the non-linear fluid modelling is coupled with the elastic deflection to provide a complete formulation to tackle EHL problems.

Finally, the integration of the proposed formulation with other linear complementarity approach that tackle the lubrication problems of the tangential velocity slip and the mixed lubrication.

The numerical implementation of the proposed formulation in the Finite Element framework is derived and discussed both in one and in two dimension.

The aim of this work is to

- establish a linear complementarity approach to the Reynolds equation for compressible, piezoviscous and non-Newtonian fluids
- couple the fluid formulation with the elastic deflection
- provide a fast and robust numerical implementation of the proposed formulation
- apply the formulation to case of practical interest, such as journal bearings

1.1 Thesis Layout

In Chapter 2 a linear complementarity formulation of the Reynolds equation for compressible, piezoviscous and non-Newtonian fluids is derived, along with a brief introduction of some rheological models commonly found in lubrication analysis. The development of the numerical implementation in the Finite Element framework of the complementarity formulation ends Chapter 2. In Chapter 3 the coupling of fluid modelling and elastic deflection is described along with the numerical implementation of the EHL formulation. Chapter 4 contains various test cases carried out to validate the proposed formulation. This Chapter ends with the detailed analysis of the journal bearing of a high performance motorsport engine. Chapter 5 shows how to combine the proposed formulation with two other linear complementarity formulation that tackle the problems of tangential velocity slip and mixed lubrication. Chapter 6 summarise this work and conclusions are drawn up.

Chapter 2

Complementarity Formulation

"Truth and clarity are complementary"

Niels Bohr

2.1 Governing Equations

2.1.1 Reynolds Equation

There are two approach available to model hydrodynamic and elastohydrodynamic lubrication problems. The first one is based on the solution of the Navier-Stokes equations and allows an accurate analysis of the fluid behaviour, at the expense of higher computational cost and complexity. The other method is based on the Reynolds equation, which is an integrated version of Navier-Stokes equation across the film thickness. This second approach has been widely employed in lubrication studies because it combines good accuracy of the solution and low computational cost.

The Reynolds equation is derived from the Navier-Stokes equations under the following assumptions:

- Inertial and body forces are negligible
- Pressure and viscosity are constant through the lubricant film
- The lubricant flow is laminar (low Reynolds number)
- No slip at the boundary surfaces

- Viscous forces are dominant, while the inertial and surface tension forces are negligible
- Shear stress and velocity gradients are only significant across the lubricant film
- The lubricant is Newtonian
- The lubricant boundary surfaces are parallel or at a small angle with respect to each other

This assumptions are usually found in common lubrication problems and, therefore, the Reynolds equation can be employed to obtain an accurate solution.

The Navier-Stokes equations allow to investigate the property of the fluid along the direction of the film thickness, whereas the Reynolds equations threat the fluid properties constant along the thickness direction.

The Reynolds equation in two dimensions is:

$$\frac{\partial}{\partial x}\left[\frac{\rho h^3}{6\mu}\frac{\partial p}{\partial x}\right]+\frac{\partial}{\partial x}\left[\frac{\rho h^3}{6\mu}\frac{\partial p}{\partial x}\right]=\frac{\partial}{\partial x}\left[\rho h(u_1+u_2)\right]+\frac{\partial}{\partial x}\left[\rho h(v_1+v_2)\right]+2\frac{\partial}{\partial t}(\rho h) \quad (2.1)$$

where ρ is the fluid density, x and y are the spatial coordinates, μ is the fluid viscosity, h is the film thickness, p is the pressure, t is time and u_1, u_2, v_1 and v_2 are the boundary surface speeds in x and y directions.

This equation deals with an isoviscous, incompressible and Newtonian fluid but it can be suitably modified in order to consider more realistic behaviours, including the variation of the viscosity as a function of pressure (piezoviscosity) and of the shear rate (non-Newtonian behaviour) and the dependency of density on pressure (compressibility).

2.1.2 Compressibility

Some well know compressibility formulations proposed in the literature to study hydrodynamic (HL) and elasto-hydrodynamic lubrication (EHL) problems are briefly summarised below.

Constant bulk modulus Probably the simplest model is based on the constant bulk modulus formulation, whereby the the following expression:

$$\beta=\rho\frac{\partial p}{\partial \rho}, \quad (2.2)$$

links the fluid bulk modulus, β, e to the pressure, p, and the density, ρ, of the lubricant. In this formulation, β is constant. Therefore, integrating once Eqn.(2.2) one obtains:

$$p = p_c \beta \ln\left(\frac{\rho}{\rho_c}\right) \Leftrightarrow \frac{\rho}{\rho_c} = e^{((p-p_c)/\beta)}, \tag{2.3}$$

where p_c is the cavitation pressure and ρ_c is the density at the cavitation pressure. This expression has been used by Vijayaraghavan and Keith [5] to analyse the behaviour of compressible fluids in finite journal bearings. However, in real lubricants, β is not constant but depends on the density of the fluid and, therefore, Eqn. (2.2) is valid only in a limited range of pressures [6].

Dowson and Higginson model A more complete formulation is the one proposed by Dowson and Higginson: [17]:

$$\frac{\rho}{\rho_c} = \frac{C_1 + C_2\,(p - p_c)}{C_1 + (p - p_c)}, \tag{2.4}$$

where C_1 and C_2 are constant coefficients, which depend on the lubricant under consideration. This compressibility formulation has been widely employed because of its good agreement with experimental results for pressure values up to 400 MPa [18]. Typical values for C_1 and C_2 are proposed in [17] where $C_1 = 0.59 \cdot 10^9$ and $C_2 = 1.34$.

Sahlin et al. [6] employed different values to best fit experimental data for mineral oil [19], namely $C_1 = 2.22 \cdot 10^9$ and $C_2 = 1.66$.

Jacobson and Vinet model Probably the most accurate expression for compressibility is the one proposed by Jacobson and Vinet [20]:

$$p = 3B_0 \left(\frac{\rho}{\rho_c}\right)^{-\frac{2}{3}} \left(1 - \frac{\left(\frac{\rho}{\rho_c}\right)^{-1}}{3}\right) e^{\left[\eta'\left(1-\left(\frac{\rho}{\rho_c}\right)^{-\frac{1}{3}}\right)\right]}. \tag{2.5}$$

This relationship shows the best results even for very high pressure values. B_0 and η' are constant parameters depending on the particular lubricant under investigation. Common values for mineral oil are $B_0 = 1.7 \cdot 10^9$ and $\eta' = 10$. Eqn.(2.5) is not analytically invertible and so a simple formula relating directly ρ and p does not exist. However, for a given pressure, a value for ρ/ρ_c can be numerically obtained employing an iterative method, such as the Newton-Raphson method [21].

This brief introduction to pressure-density relationships has shown that, at least for the considered formulations, it is possible to define a functional connection, $\rho/\rho_c = f(p)$. Therefore, by introducing this functional connection in the complementarity solver described in the previous section, any of the above formulations can be easily considered to describe the compressible behaviour of the fluid.

2.1.3 Piezoviscosity

Fluid viscosity strongly affects the performance of lubricated contacts. Experimental tests show that viscosity varies with pressure (piezoviscous effect), with temperature (thermoviscous effect) and with the shear rate (non-Newtonian behaviour). The piezoviscous effect refers to the variation of viscosity as a function of pressure. In particular as pressure increases, viscosity increases as well. In the following section, three of the most commonly employed models in HL and EHL simulations are reported.

Barus model The pressure-viscosity relationship proposed by Barus is:

$$\mu_{Barus} = \mu_0 e^{\alpha_b p} \tag{2.6}$$

where μ_0 is the viscosity at atmospheric pressure and α_b is the pressure-viscosity coefficient of the lubricant. The coefficient α_b depends on the liquid considered and does not depend on pressure. For common lubricants α_b ranges between 10^8 and $2 \cdot 10^8\, Pa^{-1}$. Although Eqn.(2.6) is widely employed, it only provides a good estimate of the viscosity for a moderate pressure range. For high pressures this exponential relationship unacceptably overestimates the viscosity value.

Roelands model Following the work by Barus, a number of empirical equations have been derived. Roelands [22] proposed the following formula based on experiment on the effect of pressure on the viscosity of lubricants under isothermal conditions:

$$\mu_{Roelands} = \mu_0 e^{\left(\alpha_p^\star p\right)} \tag{2.7}$$

where

$$\alpha_p^\star p = e^{\left\{(\ln(\mu_0)+9.67)\left[\left(1+\frac{p}{p_0}\right)^Z-1\right]\right\}} \tag{2.8}$$

Although the Roelands equation is a widely used piezoviscous model in lubricated contact problems, it again fails to model the experimentally observed piezoviscous behaviour at high pressures.

Doolittle's free-volume An alternative approach is the free volume model, which is based on the assumption that the resistance to flow in a liquid depends upon the relative volume of molecules present per unit free volume. This model combines the Tait equation of state:

$$\frac{V}{V_0} = 1 - \frac{1}{K_0' + 1} \ln \left[1 + \frac{p}{K_0} \left(1 + K_0' \right) \right] \tag{2.9}$$

and the Doolittle equation [23]

$$\mu_{Doolittle} = \mu_0 e^{\left[\beta \frac{V_{occ}}{V_0} \left(\frac{1}{\frac{V}{V_0} - \frac{V_{occ}}{V_0}} - \frac{1}{1 - \frac{V_{occ}}{V_0}} \right) \right]}, \tag{2.10}$$

where β is the Bulk modulus at $p = 0$, K_0 is the pressure rate of change of bulk modulus at $p = 0$, K_0' is the dimensionless coefficients for Poiseuille flow, V_{occ} and V_0 are the occupied volume and volume at ambient pressure respectively.

Rodermund The last formulation reported is the Rodermund equation. It has been used for the journal bearing analysis discussed in Section 4.2.

It is similar to the barus equation (Eqn.(2.6)) and it links the viscosity to the pressure using the following relationship:

$$\mu_{rodermund} = mu_0 \left(1 + a - rp \right)^{b_r} \tag{2.11}$$

2.1.4 Non-Newtonian Fluids

In lubricated contacts, piezoviscosity helps the fluid to sustain the external load, and can stabilise the motion of the components supported by the formation of the fluid film (see the piezoviscosity effects on journal bearings [24]). On the other hand, considering the numerical iterative procedure conventionally adopted to solve lubrication problems, introducing the variation of viscosity as a function of pressure could lead to a drawback: the numerical model could become unstable and, as a consequence, the solution could diverge. In fact, as a general rule, for a given film profile, the higher is the viscosity value, the higher is the pressure. Considering that the viscosity is a function of pressure in a way that an increase of pressure causes an increase of the viscosity, it can be easily understood that at high pressures this chain reaction quickly brings the pressure to grow up to infinite values, until a numerical error is returned. To overcome this undesired effect it is necessary to contain the viscosity growth rate.

One way to achieve this is to consider the shear thinning behaviour of the lubricant. Since the shear rate is affected by both the sliding speed and the pressure gradient within the fluid (see Eqn.(2.27)), this second relation has the capability to limit the pressure rise due to piezoviscosity and to stabilise the numerical solution to finite values.

Ree-Eyring According to Grieve and Spikes [25], the sinh-law equation for shear-thinning fluid proposed by Eyring is the most widely accepted:

$$\mu_{Eyring} = \frac{\tau_0}{\dot{\gamma}} \sinh^{-1}\left(\frac{\mu_0 \dot{\gamma}}{\tau_0}\right) \tag{2.12}$$

where γ is the shear rate, τ is the shear stress, μ_0 is the viscosity at ambient pressure and τ_0 represents the Newtonian limit of the lubricant, also known as Eyring stress.

Since this equation is widely accepted and employed in HL and EHD analysis, the authors decided for the usage of Eqn.(2.12) in the formulation developed, being understood that the implementation of a different shear-thinning model in the algorithm would require little additional effort.

Polynomial Shear Thinning Law The second model for shear thinning lubricant is the one adopted for the journal bearing analysis of Section 4.2.

$$\mu = \mu_0 \frac{K + \mu_\infty \dot{\gamma}}{K + \mu_0 \dot{\gamma}} \tag{2.13}$$

where μ_0 is the viscosity at $\dot{\gamma} = 0$ and μ_∞ is the asintotycal viscosity value for high shear rate ($\dot{\gamma} \to \infty$). K is a coefficient that rules the transition from μ_0 to μ_∞.

2.2 Complementarity Formulation of the Reynolds Equation for Non-Linear Fluids

In this section, a complementarity formulation of a compressible, piezoviscous and shear-thinning fluid is presented. In the definition of a complementarity algorithm, two aspects must be considered: (i) the identification of the complementary variables and (ii) the definition of the functional connection that relates them. The complementarity variables adopted here are the same as those proposed in [10], namely the pressure, p, and the void ratio (or void fraction), r, which is defined as:

$$r = 1 - \frac{\rho}{\rho_p}, \tag{2.14}$$

where ρ is the density of the mixture of oil and gases and ρ_p the density of the lubricant at the given pressure.

The complementarity formulation will be derived for a one dimensional domain for simplicity, since the same discussion can be easily extended for a two dimensional domain. The two dimensional formulation will be showed in Section 2.3.

The Reynolds equation in one dimension for unsteady and compressible flows is:

$$\frac{\partial}{\partial x}\left[\frac{\rho h^3}{6\mu}\frac{\partial p}{\partial x}\right] - 2\frac{\partial}{\partial t}\left[\rho h\right] - U\frac{\partial}{\partial x}\left[\rho h\right] = 0, \tag{2.15}$$

where h is the film thickness, U the sliding speed, and μ the fluid viscosity.

This equation is valid both in the full film region (active region) and in the cavitated (non-active) region. In the active region the lubricant is fully composed of liquid, so ρ is equal to ρ_p, while in the non-active region the fluid cavitates, becoming a mixture of liquid and vapour characterized by a density, $\rho = \rho(x, t, p)$, which is always lower than or equal to ρ_p. It follows that $(\rho_p - \rho) \geq 0$ in the whole domain. On the other hand, the pressure, p, is greater than zero in the active region and it is considered equal to the cavitation pressure in the cavitated counterpart. The pressure at which the liquid cavitates, p_c, may be taken to be zero. By this way, a sign restriction on the value of pressure p arises since $p \geq 0$ in the whole domain (note: if $p_c \neq 0$ the sign restriction applies to the difference between the fluid pressure p and the vapour pressure p_c: $p - p_c \geq 0$).

Let us define the variable ϕ as:

$$\phi = (\rho_p - \rho)\,. \tag{2.16}$$

Such variable is zero in the active region and varies in the range $0 < \phi < \rho_p$ in the non-active zone. Normalising ϕ using ρ_p, the definition of r, Eqn.(2.14), arises. Since ρ_p is strictly positive, the same considerations made for ϕ are also valid for r. From the above discussion it is evident that in the active region the pressure p is greater than zero and r is null, while in the non-active region p equals zero and r is strictly positive. Consequently, the product $p \cdot r = 0$ in the whole domain.

Therefore, the two variables p and r are complementary:

$$\begin{aligned} p &\geq 0 \\ r &\geq 0 \\ p \cdot r &= 0. \end{aligned} \tag{2.17}$$

For a compressible fluid, density is a function of pressure and it can be explicitly expressed by the general formula:

$$\rho_p = \rho_c f\left(p\right), \tag{2.18}$$

where ρ_c is the density at cavitation pressure and $f\left(p\right)$ is the functional connection between ρ_p and p.

By substitution of Eqn.(2.16) into Eqn.(2.18), it is possible to define ρ as a function of ρ_c, ϕ and $f(p)$ and to substitute it into Eqn.(2.15):

$$\begin{aligned}\frac{\partial}{\partial x}\left[\left(\rho_c f(p)-\phi\right)\frac{h^3}{6\mu}\frac{\partial p}{\partial x}\right]-2\frac{\partial}{\partial t}\left[\left(\rho_c f(p)-\phi\right)h\right]\\ -U\frac{\partial}{\partial x}\left[\left(\rho_c f(p)-\phi\right)h\right]=0.\end{aligned} \tag{2.19}$$

Rearranging Eqn.(2.19) as follows:

$$\begin{aligned}\frac{\partial}{\partial x}\left[\rho_c f(p)\left(1-\frac{\phi}{\rho_c f(p)}\right)\frac{h^3}{6\mu}\frac{\partial p}{\partial x}\right]-2\frac{\partial}{\partial t}\left[\rho_c f(p)\left(1-\frac{\phi}{\rho_c f(p)}\right)h\right]\\ -U\frac{\partial}{\partial x}\left[\rho_c f(p)\left(1-\frac{\phi}{\rho_c f(p)}\right)h\right]=0,\end{aligned} \tag{2.20}$$

and noticing that the complementarity variable r can be rewritten as:

$$r=\frac{\phi}{\rho_c f\left(p\right)}, \tag{2.21}$$

Eqn.(2.20) becomes:

$$\frac{\partial}{\partial x}\left[f(p)\left(1-r\right)\frac{h^3}{6\mu}\frac{\partial p}{\partial x}\right]-2\frac{\partial}{\partial t}\left[f(p)\left(1-r\right)h\right]-U\frac{\partial}{\partial x}\left[f(p)\left(1-r\right)h\right]=0. \tag{2.22}$$

Expanding Eqn.(2.22) one obtains:

$$\begin{aligned}\frac{\partial}{\partial x}\left[f(p)\frac{h^3}{6\mu}\frac{\partial p}{\partial x}\right]-\frac{\partial}{\partial x}\left[f(p)r\frac{h^3}{6\mu}\frac{\partial p}{\partial x}\right]-2\frac{\partial}{\partial t}\left[f(p)h\right]\\ +\frac{\partial}{\partial t}\left[f(p)rh\right]-U\frac{\partial}{\partial x}\left[f(p)h\right]+U\frac{\partial}{\partial x}\left[f(p)rh\right]=0.\end{aligned} \tag{2.23}$$

With few simple manipulations, Eqn.(2.23) can be further simplified. In particular, considering the term:

$$\frac{\partial}{\partial x}\left[f\left(p\right)r\frac{h^3}{6\mu}\frac{\partial p}{\partial x}\right], \tag{2.24}$$

the derivative of pressure $\partial p/\partial x$ equals zero in the cavitated region because the pressure is considered constant and equal to the cavitation pressure, whereas, in the active region, r, it is equal to zero. Therefore, in the whole domain, the product $(\partial p/\partial x)\cdot r = 0$ and the

term of Eqn.(2.24) can be omitted (the particular behaviour of the product $(\partial p/\partial x) \cdot r$ at the boundaries between active and cavitated regions has been already discussed in [10], which should be consulted by the interested reader).

Moreover, the terms containing the product between $f(p)$ and r can be simplified by substituting $f(p) = 1$. In fact where $r \geq 0$ (the non-active regions) $f(p) = 1$ while where $f(p) \neq 1$, $r = 0$.

Therefore, (2.23) becomes:

$$\frac{\partial}{\partial x}\left[f(p)\frac{h^3}{6\mu}\frac{\partial p}{\partial x}\right] - 2\frac{\partial}{\partial t}\left[f(p)h\right] + 2\frac{\partial}{\partial t}\left[rh\right] - U\frac{\partial}{\partial x}\left[f(p)h\right] + U\frac{\partial}{\partial x}\left[rh\right] = 0 \tag{2.25}$$

and, consequently, the complementarity formulation related to the problem of cavitation in lubricant films for compressible fluids can be defined as follows: find p and r such that:

$$\begin{gathered} \frac{\partial}{\partial x}\left[f(p)\frac{h^3}{6\mu}\frac{\partial p}{\partial x}\right] - 2\frac{\partial}{\partial t}\left[f(p)h\right] + 2\frac{\partial}{\partial t}\left[rh\right] - U\frac{\partial}{\partial x}\left[f(p)h\right] + U\frac{\partial}{\partial x}\left[rh\right] = 0 \\ p \geq 0 \\ r \geq 0 \\ p \cdot r = 0. \end{gathered} \tag{2.26}$$

This formulation allows the variation of the density of the lubricant film due to the pressure variation to be considered. It is important to emphasise that, up to this point, no assumption has been made about $f(p)$. Hence, the algorithm presented in this work allows employing *any* of the compressibility models available in the pertinent literature.

The implementation of piezoviscosity and shear thinning is briefly considered hereinafter. These two effects only modify the viscosity and, therefore, the formulation of Eqn.(2.25) can be employed without significant modifications as long as the term (2.26) is corrected to account for the changes in viscosity. In particular, μ is no longer assumed to be constant, but it is evaluated as a function of the pressure, p, and of the shear rate, γ:

$$\gamma = \frac{-h}{2\mu}\nabla p + \frac{U}{h} \tag{2.27}$$

The implementation of piezoviscosity and shear thinning is performed by modifying the viscosity that characterises the fluid at low pressures and shear rates, μ_0, introducing the dependence on the pressure in the model first, $\mu_p = \mu(p)$, followed by the shear thinning correction, which introduces the functional dependence on the shear rate, $\mu_\gamma = \mu(\gamma)$. The new viscosity value obtained, $\mu_{p,\gamma}$, is then substituted in Eqn.(2.25).

2.2.1 Functional connection between the complementarity variables

Let us consider, merely to simplify the discussion, the one dimensional steady state Reynolds equation for compressible and non isoviscous fluids in pure sliding:

$$\frac{d}{dx}\left[f\left(p\right)\frac{h^3}{6\mu_p dx}\frac{dp}{dx}\right]-U\frac{d}{dx}\left[f\left(p\right)h\right]+U\frac{d}{dx}\left[rh\right]=0. \tag{2.28}$$

Integrating Eqn.(2.28) twice with respect to x gives:

$$p=-6\mu_p U\int_0^x\frac{r}{f\left(p\right)h^2}dy+6\mu_{p,\gamma}U\int_0^x\frac{1}{h^2}dy+6\mu_p A_1\int_0^y\frac{1}{f\left(p\right)h^3}dx+A_2. \tag{2.29}$$

If we now consider the following boundary conditions:

$$p\left(0\right)=p_0;\ p\left(a\right)=p_a, \tag{2.30}$$

where a is the lubricated contact length and p_0 and p_a represent the inlet and the outlet pressure, respectively, we can easily determine the value of the constants of integration, A_1 and A_2:

$$\begin{aligned}A_1&=\frac{\left(p_a-p_0\right)-6\mu_p U\int_0^a\frac{1}{h^2}dy+6\mu_p U\int_0^a\frac{r}{f\left(p_a\right)h^2}dy}{6\mu_p\int_0^a\frac{1}{f\left(p\right)h^3}dy}\\A_2&=p_0.\end{aligned} \tag{2.31}$$

Substituting these constants back into Eqn.(2.29) gives:

$$\begin{aligned}p=&\,6\mu_p U\int_0^x\frac{1}{h^2}dy-6\mu_p U\int_0^x\frac{r}{f\left(p\right)h^2}dx\\&-\left(p_0-p_a+6\mu_p U\int_0^a\frac{1}{h^2}dy-6\mu_p U\int_0^a\frac{r}{f\left(p_a\right)h^2}dy\right)\\&\left(\int_0^x\frac{1}{f\left(p\right)h^3}dy\right)\frac{1}{\int_0^a\frac{1}{f\left(p_a\right)h^3}dy}+p_0\end{aligned} \tag{2.32}$$

Eqn.(2.28) can be rewritten in the following compact functional form:

$$p=Lr+Q, \tag{2.33}$$

where L represents the operator relating the complementarity variables p and r, and Q is the term that carries the information about the boundary conditions of the problem and the shape of the lubricant film thickness.

The linear complementarity problem of Eqn. (2.33) can be solved numerically using the Galerkin method in the Finite Element framework [26]. In this work, a similar approach to the one described in [10] has been used along with a specific formulation for the derivation of $f(p)$ and $\mu_{p,\gamma}$. In particular, a semi-implicit algorithm has been adopted to derive the values of density and viscosity.

2.3 Numerical Implementation

"Numbers exist only in our minds. There is no physical entity that is number 1. If there were, 1 would be in a place of honor in some great museum of science, and past it would file a steady stream of mathematicians gazing at 1 in wonder and awe."

Fraleigh/Beauregard, Linear Algebra

In this section, the Finite Element implementation of the formulation presented in the section 2.2 is derived for a two dimensional domain.

$$\begin{aligned}\frac{\partial}{\partial x}\left[f(p)\frac{h^3}{6\mu}\frac{\partial p}{\partial x}\right]\frac{\partial}{\partial y}\left[f(p)\frac{h^3}{6\mu}\frac{\partial p}{\partial y}\right]-2\frac{\partial}{\partial t}\left[f(p)h\right]+2\frac{\partial}{\partial t}\left[rh\right]\\ -U\frac{\partial}{\partial x}\left[f(p)h\right]+U\frac{\partial}{\partial x}\left[rh\right]-U\frac{\partial}{\partial y}\left[f(p)h\right]+U\frac{\partial}{\partial y}\left[rh\right]=0\end{aligned} \tag{2.34}$$

Eqn.(2.34), can be solved numerically using the Galerkin method:

$$\begin{aligned}\int_\Omega W\left[\frac{\partial}{\partial x}\left(f(p)\frac{h^3}{6\mu_{p,\gamma}}\frac{\partial p}{\partial x}\right)+\frac{\partial}{\partial y}\left(f(p)\frac{h^3}{6\mu_{p,\gamma}}\frac{\partial p}{\partial y}\right)-2\frac{\partial}{\partial t}\left(f(p)h\right)\right.\\ \left.+2\frac{\partial}{\partial t}\left(rh\right)-U_x\frac{\partial}{\partial x}\left(f(p)h\right)-U_y\frac{\partial}{\partial y}\left(f(p)h\right)+U_x\frac{\partial}{\partial x}\left(rh\right)+U_y\frac{\partial}{\partial y}\left(rh\right)\right]d\Omega=0\end{aligned} \tag{2.35}$$

where W is the test function.

Separation of the individual terms of Eqn.(2.35) gives:

$$\begin{aligned}\int_\Omega W\frac{\partial}{\partial x}\left(f(p)\frac{h^3}{6\mu_{p,\gamma}}\frac{\partial p}{\partial x}\right)d\Omega+\int_\Omega W\frac{\partial}{\partial y}\left(f(p)\frac{h^3}{6\mu_{p,\gamma}}\frac{\partial p}{\partial y}\right)d\Omega-\int_\Omega W2\frac{\partial}{\partial t}\left(f(p)h\right)d\Omega\\ +\int_\Omega W2\frac{\partial}{\partial t}\left(rh\right)d\Omega-\int_\Omega WU_x\frac{\partial}{\partial x}\left(f(p)h\right)d\Omega-\int_\Omega WU_y\frac{\partial}{\partial y}\left(f(p)h\right)d\Omega\\ +\int_\Omega WU_x\frac{\partial}{\partial x}\left(rh\right)d\Omega+\int_\Omega WU_y\frac{\partial}{\partial y}\left(rh\right)d\Omega=0.\end{aligned} \tag{2.36}$$

When evaluating the diffusion terms, an integration by parts is generally introduced:

$$\int_\Omega W\frac{\partial}{\partial x}\left(f(p)\frac{\rho h^3}{6\mu_{p,\gamma}}\frac{\partial p}{\partial x}\right)d\Omega = W\left(f(p)\frac{h^3}{6\mu_{p,\gamma}}\frac{\partial p}{\partial x}\right)\Big|_{\Omega_0} - \int_\Omega f(p)\frac{h^3}{6\mu_{p,\gamma}}\frac{\partial W}{\partial x}\frac{\partial p}{\partial x}d\Omega. \tag{2.37}$$

$$\int_\Omega W\frac{\partial}{\partial y}\left(f(p)\frac{\rho h^3}{6\mu_{p,\gamma}}\frac{\partial p}{\partial y}\right)d\Omega = W\left(f(p)\frac{h^3}{6\mu_{p,\gamma}}\frac{\partial p}{\partial y}\right)\Big|_{\Omega_0} - \int_\Omega f(p)\frac{h^3}{6\mu_{p,\gamma}}\frac{\partial W}{\partial y}\frac{\partial p}{\partial y}d\Omega. \tag{2.38}$$

These integrations by parts lead to a weak form of Eqn.(2.35) The two first right hand side terms of Eqn.(2.37) and Eqn.(2.38) should be evaluated on the domain boundaries. However, these terms can be neglected because a pressure value is usually prescribed along these boundaries [27]. Eqn.(2.36) becomes:

$$\begin{aligned} &-\int_\Omega \frac{f(p)h^3}{6\mu_{p,\gamma}}\frac{\partial W}{\partial x}\frac{\partial p}{\partial x}d\Omega - \int_\Omega \frac{f(p)h^3}{6\mu_{p,\gamma}}\frac{\partial W}{\partial y}\frac{\partial p}{\partial y}d\Omega - \int_\Omega W2\frac{\partial}{\partial t}\left(f(p)h\right)d\Omega \\ &+\int_\Omega W2\frac{\partial}{\partial t}\left(rh\right)d\Omega - \int_\Omega WU_x\frac{\partial}{\partial x}\left(f(p)h\right)d\Omega - \int_\Omega WU_y\frac{\partial}{\partial y}\left(f(p)h\right)d\Omega \\ &+\int_\Omega WU_x\frac{\partial}{\partial x}\left(rh\right)d\Omega + \int_\Omega WU_y\frac{\partial}{\partial y}\left(rh\right)d\Omega = 0. \end{aligned} \tag{2.39}$$

Then, the lubrication domain can be divided into a finite number of elements and Eqn.(2.39) can be discretized and solved over each element domain Ω_e.

Using proper shape functions N_i, a general variable ϕ can be interpolated inside each element as

$$\phi \approx \sum_{i=1}^{N_n} N_i\tilde{\phi}_i \tag{2.40}$$

where N_n is the number of nodes per element, N_i is the shape function and $\tilde{\phi}_i$ is the value of the variable ϕ at node i. For a two-dimensional problem, bilinear shape functions can be used:

$$\begin{aligned} N_1 &= (1-\xi)(1-\eta)\frac{1}{4} \\ N_2 &= (1+\xi)(1-\eta)\frac{1}{4} \\ N_3 &= (1+\xi)(1+\eta)\frac{1}{4} \\ N_4 &= (1-\xi)(1+\eta)\frac{1}{4} \end{aligned} \tag{2.41}$$

where ξ and η are the element local coordinates.

As a consequence, the derivative of an interpolated function ϕ is given in terms of its nodal values as:

$$\frac{\partial \phi}{\partial x} \approx \sum_{i=1}^{N_n} \frac{\partial N_i}{\partial x} \tilde{\phi}_i. \tag{2.42}$$

Employing the Gaussian quadrature rule for the numerical integration, the discretized form of Eqn.(2.39) on the general j-th node of the element Ω_e becomes:

$$\begin{aligned} F_j\left(\Omega_e\right) = & -\sum_{m=1}^{N_{gp}} \left[\sum_{k=1}^{N_n} \frac{1}{6\mu_m} h_m^3 f(p)_m \left(\frac{\partial N_{mk}}{\partial x} \frac{\partial W_{mj}}{\partial x} + \frac{\partial N_{mk}}{\partial y} \frac{\partial W_{mj}}{\partial y} \right) p_k \right] w_m \Delta\Omega_m \\ & + \sum_{m=1}^{N_{gp}} \left[\sum_{k=1}^{N_n} W_{mj} \left(\frac{\partial N_{mk}}{\partial x} r_k h_k \right) \left(U_x + U_y \right) \right] w_m \Delta\Omega_m \\ & - \sum_{m=1}^{N_{gp}} \left[W_{mj} \frac{\partial}{\partial x} \left(f\left(p\right)_m h_m \right) \left(U_x + U_y \right) \right] w_m \Delta\Omega_m \\ & + \frac{2}{\Delta t} \sum_{m=1}^{N_{gp}} \left[\sum_{k=1}^{N_n} W_{mj} N_{mk} \left(r_k\left(t\right) h_k\left(t\right) - r_k\left(t-\Delta t\right) h_k\left(t-\Delta t\right) \right) \right] w_m \Delta\Omega_m \\ & - \frac{2}{\Delta t} \sum_{m=1}^{N_{gp}} \left[W_{mj} f\left(p\left(t\right)\right)_m \left(h_m\left(t\right) - h_m\left(t-\Delta t\right) \right) \right] w_m \Delta\Omega_m = 0. \end{aligned} \tag{2.43}$$

where the m-index defines a general Gauss point, w_m is the corresponding weight, $\Delta\Omega_m$ is the determinant of the coordinate transformation from the global coordinate system to the local element coordinate system, the k-index defines a general element node and N_{gp} and N_n represent the number of Gauss points and nodes for each element, respectively.

Writing Eqn.(2.43) for each node of the domain, a system of non-linear algebraic equations is obtained in the following form:

$$[A]\, p + [B]\, r + C = 0, \tag{2.44}$$

where:

$$A_{j,k} = -\sum_{n=1}^{N_e} \left\{ \sum_{m=1}^{N_{gp}} \left[\sum_{k=1}^{N_n} \frac{1}{6\mu_m} h_m^3 f(p_{i-1})_m \left(\frac{\partial N_{mk}}{\partial x} \frac{\partial W_{mj}}{\partial x} + \frac{\partial N_{mk}}{\partial y} \frac{\partial W_{mj}}{\partial y} \right) \right] w_m \Delta\Omega_m \right\} \tag{2.45}$$

$$\begin{aligned} B_{j,k} = \sum_{n=1}^{N_e} \Bigg\{ \sum_{m=1}^{N_{gp}} \Bigg[& U_x \sum_{k=1}^{N_n} W_{mj} h_k \left(\frac{\partial N_{mk}}{\partial x} \right) + U_y \sum_{k=1}^{N_n} W_{mj} h_k \left(\frac{\partial N_{mk}}{\partial y} \right) \\ & + 2 \frac{1}{\Delta t} \sum_{k=1}^{N_n} W_{mj} N_{mk} h_k(t) \Bigg] w_m \Delta\Omega_m \Bigg\} \end{aligned} \tag{2.46}$$

$$C_j = -\sum_{n=1}^{N_e}\left\{\sum_{m=1}^{N_{gp}}\left[U_x W_{mj}\frac{\partial}{\partial x}\left(f(p_{i-1})_m h_m\right) + U_y W_{mj}\frac{\partial}{\partial y}\left(f(p_{i-1})_m h_m\right)\right]\right.$$
$$\left. + \left[2W_{mj} f(p_{i-1})_m \frac{h_m(t) - h_m\left(t-\Delta t\right)}{\Delta t} + \frac{2}{\Delta t} W_{mj}\sum_{k=1}^{N_n}\left[N_{mk} r_k\left(t-\Delta t\right) h_k\left(t-\Delta t\right)\right]\right] w_m \Delta\Omega_m\right\}. \tag{2.47}$$

Consider the matrix $[A]$, which derives from the discretization of the Poiseuille term within the Reynolds equation, Eqn. (2.25). After imposing the boundary conditions in terms of pressure and by inverting matrix $[A]$, one obtains:

$$p = -\left[A\right]^{-1}\left[B\right] r - \left[A\right]^{-1} C \rightarrow p = \left[L\right] r + Q, \tag{2.48}$$

where

$$\left[L\right] = -\left[A\right]^{-1}\left[B\right] \text{ and } Q = -\left[A\right]^{-1} C. \tag{2.49}$$

The system of algebraic equations (2.48) can now be solved using a suitable pivoting algorithm for complementarity problems. The value of pressure used to evaluate the compressibility function $f\left(p\right)$ and the viscosity $\mu_{p,\gamma}$ is the one obtained from the solution of the previous iteration. Therefore, the derived formulation results in a semi-implicit method that can be solved using an iterative Newton-Raphson method.

Particular care has to be devoted in the selection of appropriate test functions for the terms of Eqn.(2.46). In fact, undesired oscillations may arise in the solution for r, because of the hyperbolic character of the equation to be solved in the cavitated region. A commonly employed method is to choose as test functions appropriate decentred polynomial functions[26]:

$$W_i = N_i + \alpha\frac{dN_i}{dx}\text{sign}(U) \tag{2.50}$$

with α that ranges from 0 (standard Galerkin approximation) to 1 (full upwind discrete equation) and sign(U) gives the velocity direction for terms of Eqn.(2.46) containing U_x and U_y.

Other existing methods consist in properly modifying the integration points used for the numerical evaluation of the integrals of the terms containing the variable r [28]. In the numerical algorithm developed the author preferred the second method because considers it more elegant and because it reduces the number of numerical operation to assembly the matrix of Eqn.(2.46). In particular the shape functions N_i are employed as test functions W_i. Then, all the terms of Eqn.(2.46) are integrated using integration points (ξ_{int}, η_{int}) different than the standard gauss points $(\xi_{gauss}, \eta_{gauss})$.

The formulation for a one dimensional domain can be derived from the one discussed above by setting to zero all the terms that depends on the y coordinate: U_y, $\partial h/\partial y$, $\partial N/\partial y$ and $\partial W/\partial y$. For this case the shape functions can be taken as linear:

$$\begin{aligned} N_1 &= (1-\xi)\,\frac{1}{2} \\ N_2 &= (1+\xi)\,\frac{1}{2}. \end{aligned} \tag{2.51}$$

The integration point and its corresponding weight to be employed for the numerical integration of the terms of Eqn.(2.46) are:

$$m = \xi_{int}, \quad w = 2 \tag{2.52}$$

where ξ_{int} ranges from 0 to 1.

Fig.2.1 compares the solutions in term of p and r for different values of α and ξ_{int}. Best results are obtained considering $\xi_{int} = 1$ and $\alpha = 1$. No numerical difference in the solution between the two approach appears.

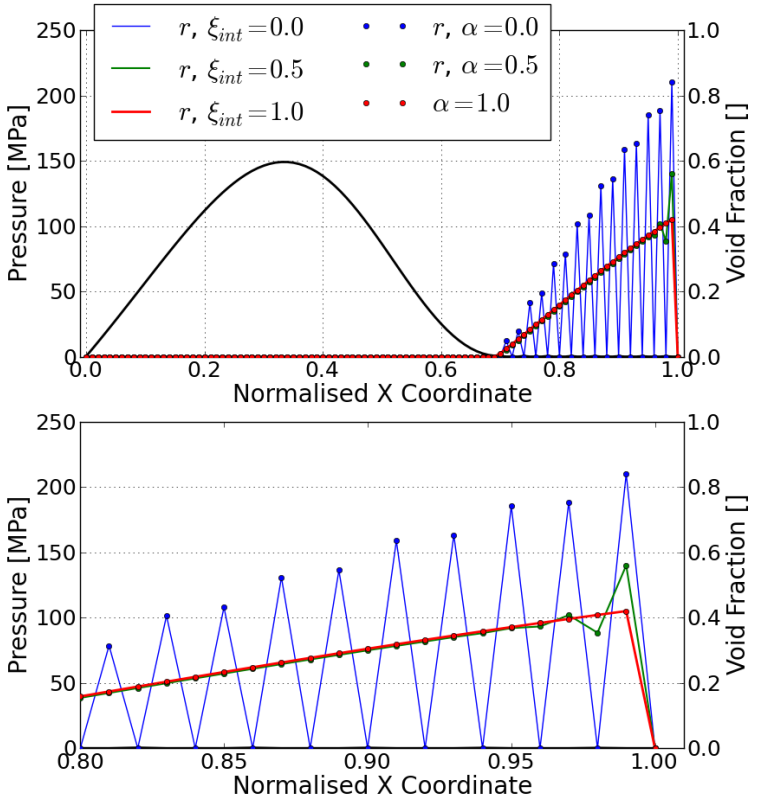

FIGURE 2.1: a) Comparison of the solutions of the problem in 4.1.1 in terms of p and r using different integration points ξ_{int} and different upwind parameter α for the terms of Eqn.(2.46) and b) detail of the different solutions for r in the cavitated region

Chapter 3

Elastic Deflection

3.1 Governing Equations

In the case of rigid surfaces, the geometry of the two mating bodies entirely defines the film thickness, h, to be used in the Reynolds equation, Eqn.(2.26). This consideration is no longer valid in the case of the solid bodies being elastic. In fact, in this case the total film thickness is the sum of the geometric thickness plus the elastic deflection.

Fig.3.1 depicts the film thickness and the main symbols employed. h_g is the geometric thickness, that is the film thickness in the case of rigid bodies, and h_e is the deflection of the solid surfaces due to the fluid pressure. The deflection h_e is assumed to be elastic.

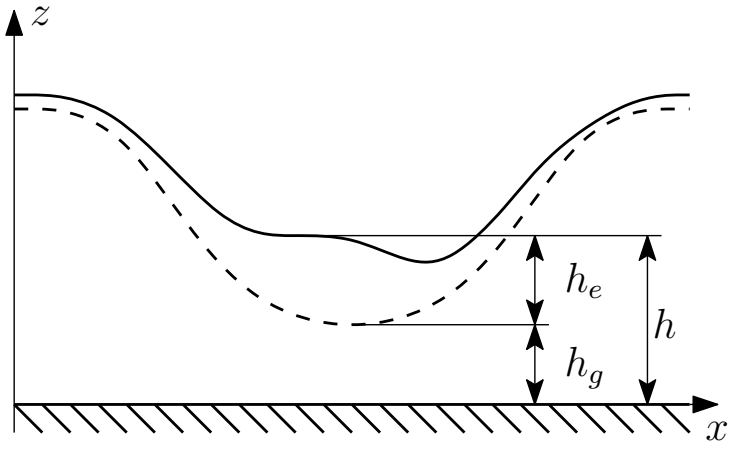

FIGURE 3.1: The two contribution to the total film thickness

The total film thickness, h, is given by the sum of the undeformed geometry, h_g, and the elastic deflection, h_e:

$$h = h_g + h_e, \tag{3.1}$$

3.1.1 Elastic Deflection

The interaction between the fluid and the solid domains in EHL formulations can be expressed in term of normal stress and shear stress. The effects of the shear stress on the deformed shape of the journal are considered negligible. Therefore, the only contribution to the elastic deflection is given by the normal stresses.

The deformation in an elastohydrodynamic contact can be calculated (i) using the Hertzian theory of elastic contact or (ii) using ad-hoc Finite Element models of the problem under investigation. The Hertzian theory of contact, (i), provides a more general approach to contact problems that can be applied for a wide range of geometries. On the other hand, the Finite Element modelling, (ii), allows to simulate a specific problem more accurately. In order to do so, an external software to create the discretized model of the solid bodies and to extract the compliance matrix is required.

It is important to point out that there is no difference in the following EHL formulation, whatever is the technique chosen for the evaluation of the elastic deflection.

3.1.1.1 Hertzian theory

From the Hertzian theory, [29], the elastic deflection, w, is given by:

$$w\left(x,y\right) = \frac{1}{E_r} \iint\limits_A \frac{p\left(x_1,y_1\right)}{\sqrt{\left(x-x_1\right)^2 + \left(y-y_1\right)^2}} dx_1 dy_1 \tag{3.2}$$

where p is the fluid pressure at coordinates (x_1, y_1) that acts on an area $dx_1 dy_1$. E_r is the reduced Young's Modulus:

$$\frac{1}{E_r} = \frac{1}{\pi}\left(\frac{1-{\nu_1}^2}{E_1} + \frac{1-{\nu_2}^2}{E_2}\right) \tag{3.3}$$

where $E_{1,2}$ are the Young's moduli and $\nu_{1,2}$ are the Poisson's ratios of the two bodies.

The assumptions underlying the Hertzian contact theory are:

- The radii of curvature of the contacting bodies are large compared with the radius or width of the contact area.

- The dimensions of each body are large compared to the radius of the circle of contact.
- The contact is frictionless.
- The surfaces in contact are continuous and nonconforming.
- The materials are elastic and isotropic.

For a one dimensional domain, considering the pressure constant over each element, the relation between the deflection at the node i caused by the pressure on a surface element j is provided in [30] and it is:

$$h_{e,ij} = \frac{p_j}{E_r}\left[4c_j \ln(2b) + (d_{ij} - c_j)\ln(d_{ij} - c_j)^2 - (d_{ij} + c_j)\ln(d_{ij} + c_j)^2\right] \tag{3.4}$$

where c_j is the half-width of the element and d_{ij} is the distance between the node i and the centre of the element j. In [30] it is possible also to find the equation for two dimensional problems. A complete discussion of the Hertzian contact theory is out of the scope of this thesis and can be found in [29], to which the interested reader is referred.

3.1.1.2 Finite Element contact model

If we consider a constrained body, that is a body with no rigid body motions, it is possible to extract the compliance matrix of the contact nodes via static reduction of the complete stiffness matrix [1]. The equation governing the static problem ($\ddot{x} = \dot{x} = 0$) reduces to:

$$[K]\bar{x} = [F] \tag{3.5}$$

Figure 3.2 sketches the FE models of two bodies in contact: A and B. For each body there is a subset of nodes, b_A and b_B, which are the boundary nodes and are marked in red. The interior nodes, i_A and i_B, are depicted in blue.

Consider the stiffness matrix K_A of the contact body A. It is possible to partition the stiffness matrix as follows:

$$K_A = \begin{bmatrix} K_{bb} & K_{bi} \\ K_{ib} & K_{ii} \end{bmatrix} \begin{vmatrix} x_b \\ x_i \end{vmatrix} = \begin{vmatrix} F_b \\ F_i \end{vmatrix} \tag{3.6}$$

where the subscript b refers to the boundary nodes and the subscript i to the itnerior nodes.

[1] The stiffness matrix has to be calculated with an external procedure for structural Finite Element analysis.

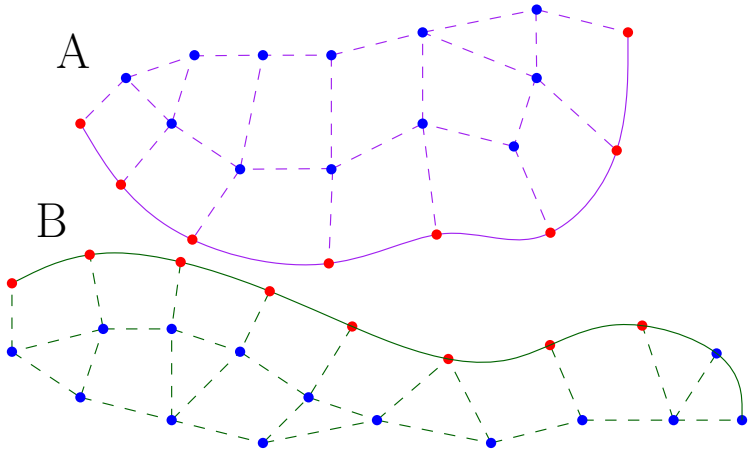

FIGURE 3.2: Schematic of two contact bodies. The red nodes are contact (boundary) nodes while the blue ones are interior nodes

If the bodies are at rest and the only load applied to the system is the contact force, it follows that the external force on the inner nodes is:

$$\bar{F}_i = 0. \tag{3.7}$$

Moreover, only x_b is desired. Writing out the set of equations from Eqn.(3.6):

$$\begin{cases} K_{bb}x_b + K_{bi}x_i = F_b \\ K_{ib}x_b + K_{ii}x_i = 0. \end{cases} \tag{3.8}$$

The second equation can be rearranged as:

$$-K_{ii}^{-1}K_{ib}x_b = x_i. \tag{3.9}$$

Substituting Eqn.(3.9) into Eqn.(3.8)

$$K_{bb}x_b - K_{bi}K_{ii}^{-1}K_{ib}x_b = F_b. \tag{3.10}$$

In matrix form:

$$\left[K_{red,A}\right]\bar{x}_b = \bar{F}_b \tag{3.11}$$

where:

$$K_{red,A} = K_{bb} - K_{bi}K_{ii}^{-1}K_{ib} \tag{3.12}$$

Note the matrix inversion. This requires a non-singular stiffness sub-matrix.

The matrix $K_{red,A}$ has to be inverted to obtain the compliance matrix C_A that links the forces to the deformations between the contact nodes.

$$C_A = K_{red,A}^{-1}. \tag{3.13}$$

The compliance matrices of the two touching bodies are summed element-wise to obtain the total compliance:

$$C = C_A + C_B. \tag{3.14}$$

3.2 Numerical Implementation

In a discretized domain, it is possible to evaluate the elastic deflection at every points of the domain by interpolation of the nodal values with proper shape functions. The shape functions can be taken as shown in Eqn.(2.40).

The values of the nodal displacement is obtained by multiplication of the compliance matrix of the domain, C, with the pressure field, $\bar{p}$:

$$\bar{h}_e = [C] \cdot \bar{p} \tag{3.15}$$

The sum of the elastic deflection h_e with the geometric thickness h_g gives the total film thickness h (Eqn.3.1).

The EHL complementarity formulation of the Reynolds equation in the case of cavitation for compressible, piezoviscous and non-Newtonian lubricant becomes: find p and r such that

$$\begin{aligned} \frac{\partial}{\partial x}\left[f(p)\frac{h^3}{6\mu}\frac{\partial p}{\partial x}\right]\frac{\partial}{\partial y}\left[f(p)\frac{h^3}{6\mu}\frac{\partial p}{\partial y}\right] - 2\frac{\partial}{\partial t}\left[f(p)h\right] + 2\frac{\partial}{\partial t}\left[rh\right] \\ -U\frac{\partial}{\partial x}\left[f(p)h\right] + U\frac{\partial}{\partial x}\left[rh\right] - U\frac{\partial}{\partial y}\left[f(p)h\right] + U\frac{\partial}{\partial y}\left[rh\right] = 0 \\ h = h_g + \ell p \\ p \geq 0 \\ r \geq 0 \\ p \cdot r = 0. \end{aligned} \tag{3.16}$$

where ℓ is the linear integral operator that gives the elastic deflection of the solid surfaces due to the pressure (in a discretized geometry ℓ is represented by the compliance matrix, C).

The non-linear nature of the coupling of the Reynolds and the elastic equations requires the implementation of a iterative procedure. At each iteration, the film thickness is evaluated with Eqn.(3.1) and Eqn.(3.15) using the previous pressure solution, then the Reynolds equation in terms of p and r is solved. This procedure loops until the satisfaction of suitable convergence criteria.

This simple explicit method is not appropriate for the highly non-linear behaviour of the system of equation that describe - the EHL problem. Convergence issues arise and proper under-relaxation factors are required. The introduction of under-relaxation increases the computational cost and the time require to obtain the numerical solution. Moreover, the convergence is not guaranteed.

A suitable flavour of the Newton method, that will be discussed in the following, has been introduced to tackle this problem.

3.2.1 Newton method for EHL problems

"Anyone who cannot cope with mathematics is not fully human. At best he is a tolerable sub-human who has learned to wear shoes, bathe, and not make messes in the house."

Robert Heinlein, Time Enough For Love

To unfold the mathematical theory of the Newton method applied to the EHL problem, we will start again with the Reynolds equation in one dimension for incompressible and isoviscous fluids. These restrictions are made for brevity, but the same outline can be followed with the Reynolds equation for a compressible, piezoviscous and shear thinning lubricant.

This equation is coupled with the elastic deflection equation. This set of equations is:

$$\begin{cases} \dfrac{\partial}{\partial x}\left[\dfrac{h^3}{6\mu}\dfrac{\partial p}{\partial x}\right] - 2\dfrac{\partial h}{\partial t} + 2\dfrac{\partial rh}{\partial t} - U_x\dfrac{\partial h}{\partial x} + U_x\dfrac{\partial rh}{\partial x} = 0 \\ h = h_g + \ell p \end{cases} \tag{3.17}$$

Following the Rohde's formulation [31], the system of equation can be written as non-linear integrodifferential operator equation for p

$$F(p) = 0. \tag{3.18}$$

An iterative procedure has to be set to solve Eqn.(3.18). At each step h is evaluated with the pressure distribution p_s of the previous step. The solution of the first equation

of Eqn.(3.17) gives the new pressure distribution p_{s+1}. This iterative procedure does not guarantee the convergence of the pressure solution.

It is possible, instead, to use Newton's method to obtain at each step a better distribution p_{s+1}.

$$F(p_s) + F'(p_s)\epsilon_s = 0. \tag{3.19}$$

F' is the functional derivative of F and ϵ is the error $\epsilon = p_{s+1} - p_s$. The functional derivative is defined by

$$F'(p)\epsilon = \frac{d}{d\delta}F(p+\delta\epsilon)\bigg|_{\delta=0} \tag{3.20}$$

where F' is the functional derivative, or Frchet derivative. The derivation of the functional derivative follows.

The combination of the two equations of the set of Eqn.(3.17) yields:

$$\frac{\partial}{\partial x}\left[\frac{(h_g+\ell p)^3}{6\mu}\frac{\partial p}{\partial x}\right] - 2\frac{\partial}{\partial t}(h_g+\ell p) + 2\frac{\partial}{\partial t}[r(h_g+\ell p)] - U_x\frac{\partial}{\partial x}(h_g+\ell p) + U_x\frac{\partial}{\partial x}[r(h_g+\ell p)]. \tag{3.21}$$

Now the functional derivative of the EHL Reynolds equation can be expressed substituting Eqn.(3.21) in Eqn. (3.20).

$$\begin{aligned} F'(p_s)\epsilon = \frac{d}{d\delta}\Bigg[\frac{\partial}{\partial x}\Bigg[\frac{(h_g+\ell(p_s+\delta\epsilon))^3}{6\mu}\frac{\partial(p_s+\delta\epsilon))}{\partial x}\Bigg] \\ -2\frac{\partial}{\partial t}(h_g+\ell p_s+\delta\epsilon)) + 2\frac{\partial}{\partial t}[r(h_g+\ell(p_s+\delta\epsilon))] \\ -U_x\frac{\partial}{\partial x}(h_g+\ell(p_s+\delta\epsilon)) + U_x\frac{\partial}{\partial x}[r(h_g+\ell(p_s+\delta\epsilon))]\Bigg]\Bigg|_{\delta=0} \end{aligned} \tag{3.22}$$

Deriving with respect to δ:

$$\begin{aligned} \frac{1}{6\mu}\frac{d}{dx}\left[3\ell(\epsilon)\left(\ell(p)+h_g+\ell(\delta\epsilon)\right)^2\frac{d}{dx}(p+\delta\epsilon) + \frac{d\epsilon}{dx}\left(\ell(p)+h_g+\ell(\delta\epsilon)\right)^3\right] \\ U\frac{d}{dx}[\ell(\epsilon)r] - U\frac{d}{dx}[\ell(\epsilon)] + 2\frac{d}{dt}[\ell(\epsilon)r] - 2\frac{d}{dt}[\ell(\epsilon)] \end{aligned} \tag{3.23}$$

and putting $\delta = 0$, given that $\ell(0) = 0$:

$$\begin{aligned} \frac{1}{6\mu}\frac{d}{dx}\left[3\ell(\epsilon)\left(\ell(p)+h_g\right)^2\frac{d}{dx}(p) + \frac{d\epsilon}{dx}\left(\ell(p)+h_g\right)^3\right] \\ U\frac{d}{dx}[\ell(\epsilon)r] - U\frac{d}{dx}[\ell(\epsilon)] + 2\frac{d}{dt}[\ell(\epsilon)r] - 2\frac{d}{dt}[\ell(\epsilon)] \end{aligned} \tag{3.24}$$

The substitution of Eqn.(3.24) into Eqn.(3.19) yields:

$$+\frac{1}{6\mu}\frac{\partial}{\partial x}\left[(\ell(p_s)+h_g)^3\frac{\partial}{\partial x}(p_s+\epsilon)\right]+\frac{1}{6\mu}\frac{\partial}{\partial x}\left[3\left(\ell(p_s)+h_g\right)^2\ell(p+\epsilon)\frac{\partial p_s}{\partial x}\right]$$
$$-\frac{1}{6\mu}\frac{\partial}{\partial x}\left[3\ell(p_s)\left(\ell(p_s)+h_g\right)^2\frac{\partial p_s}{\partial x}\right]+U\frac{\partial}{\partial x}\left[(\ell(p_s+\epsilon)+h_g)r\right]-U\frac{\partial}{\partial x}\left[\ell(p_s+\epsilon)+h_g\right]$$
$$+2\frac{\partial}{\partial t}\left[(\ell(p_s+\epsilon)+h_g)r\right]-2\frac{\partial}{\partial t}\left[\ell(p_s+\epsilon)+h_g\right]=0. \tag{3.25}$$

The following substitution are made: $p_s+\epsilon=p_{s+1}$, $\ell(p_s)+g=h_s$ and $\ell(p_s)=h_{e,s}$. Eqn.(3.25) defines a linear integrodifferential equation for the new pressure distribution p_{s+1} and void fraction r_{s+1} as a function of the undeformed film thickness h_g, the total thickness and the elastic deflection evaluated at the previous step, h_s and $h_{e,s}$ respectively:

$$+\frac{1}{6\mu}\frac{\partial}{\partial x}\left[h_s^3\frac{\partial p_{s+1}}{\partial x}\right]+\frac{1}{6\mu}\frac{\partial}{\partial x}\left[3h_s^2\ell(p_{s+1})\frac{\partial p_s}{\partial x}\right]-\frac{1}{6\mu}\frac{\partial}{\partial x}\left[3h_{e,s}h_s^2\frac{\partial p_s}{\partial x}\right]$$
$$+U\frac{\partial}{\partial x}\left[(\ell(p_{s+1})+h_g)r\right]-U\frac{\partial}{\partial x}\left[\ell(p_{s+1})+h_g\right]+2\frac{\partial}{\partial t}\left[(\ell(p_{s+1})+h_g)r\right]-2\frac{\partial}{\partial t}\left[\ell(p_{s+1})+h_g\right]=0. \tag{3.26}$$

This approach was first derived by Rhode in [31] and its difference with more conventional methods is that it incorporates both the hydrodynamic and the elastic equation in a single expression. In this way, the iterative stability problems that arise treating separately the two equation are overcome. A clear and more detailed discussion on the advantages of this approach is presented in [32].

Eqn.(3.26) allows to evaluate a better approximation for p_{s+1} with respect to standard explicit methods. However, when convergence is reached, p and r are still solution to the Reynolds equation, because when $\epsilon=0$, $p_{s+1}=p_s$ and Eqn.(3.26) degenerate in the Reynolds equation. It is interesting to note that this occurs also for rigid solid surfaces ($\ell=0$).

It is important to highlight that Eqn.(3.26) is no more linear on the two complementary variables p_{s+1} and r because of the products $\ell(p_{s+1})\cdot r$. To preserve the advantages of the linear complementarity approach it is possible to consider $\ell(p_{s+1})$ equals to $\ell(p_s)$ in the terms of Eqn.(3.26) that contain r. This modification, obviously, does not affect the final solution of the numerical procedure. At the same time, the number of iteration needed does not increase because of the linear dependency of the solution on the variable r.

3.2.2 Finite Element discretization of the EHL Reynolds equation

"As a matter of fact, once the problem has been well defined it is inevitable that the solution, approximated or exact, will be found."

Carlo Maria Cipolla

In this section the discretization in the Finite Element framework of the Reynolds equation for EHL problems is discussed. The same outline of section 2.3 is followed.

The multiplication of Eqn.(3.26) by a test function W yields:

$$\begin{aligned}\int_\Omega W \Bigg[\frac{1}{6\mu}\frac{\partial}{\partial x}\left[h_s^3\frac{\partial p_{s+1}}{\partial x}\right] + \frac{1}{6\mu}\frac{\partial}{\partial x}\left[3h_s^2\ell(p_{s+1})\frac{\partial p_s}{\partial x}\right] - \frac{1}{6\mu}\frac{\partial}{\partial x}\left[3h_{e,s}h_s^2\frac{\partial p_s}{\partial x}\right] \\ +U\frac{\partial}{\partial x}\left[(\ell(p_{s+1})+h_g)r\right] - U\frac{\partial}{\partial x}\left[\ell(p_{s+1})+h_g\right] \\ +2\frac{\partial}{\partial t}\left[(\ell(p_{s+1})+h_g)r\right] - 2\frac{\partial}{\partial t}\left[\ell(p_{s+1})+h_g\right]\Bigg] d\Omega = 0.\end{aligned} \tag{3.27}$$

Eqn.(3.27) is expanded and the term containing the second derivative in p is integrated by parts. The same considerations discussed for Eqn.(2.37) are made, thus Eqn.(3.27) becomes:

$$\begin{aligned}-\int_\Omega \frac{f(p)h_s^3}{6\mu}\frac{\partial W}{\partial x}\frac{\partial p_{s+1}}{\partial x}d\Omega - \int_\Omega \frac{f(p)h_s^2}{6\mu}\ell(p_{s+1})\frac{\partial W}{\partial y}\frac{\partial p_s}{\partial y}d\Omega \\ -\int_\Omega \frac{f(p)h_s}{6\mu}h_{e,s}^2\frac{\partial W}{\partial y}\frac{\partial p_s}{\partial y}d\Omega + \int_\Omega WU\frac{\partial}{\partial x}\left[(\ell(p_{s+1})+h_g)r\right]d\Omega \\ -\int_\Omega WU\frac{\partial}{\partial x}\left[\ell(p_{s+1})+h_g\right]d\Omega + \int_\Omega W2\frac{\partial}{\partial t}\left[(\ell(p_{s+1})+h_g)r\right]d\Omega \\ -\int_\Omega W2\frac{\partial}{\partial t}\left[\ell(p_{s+1})+h_g\right]d\Omega = 0.\end{aligned} \tag{3.28}$$

where the other term that derives from the integration by parts is neglected because a fixed pressure, or a fixed void fraction, is prescribed at the boundaries.

A discretized domain is introduced. The values of the lubricant and solid properties are evaluated at the nodes of the numerical grid, whereas the values of the properties inside each element of the domain is obtained by interpolation of the nodal values using the shape functions of Eqn.(2.41). The variables derivative are calculated with Eqn.(2.42)

The Gauss quadrature rule is employed for the numerical integration. The discretized form of Eqn.(3.28) on the general j-th node of the element Ω_e is:

$$\begin{aligned}
F_j\left(\Omega_e\right) = & -\sum_{m=1}^{N_{gp}}\left[\sum_{k=1}^{N_n}\frac{1}{6\mu_m}h_m^3\left(\frac{\partial N_{mk}}{\partial x}\frac{\partial W_{mj}}{\partial x}\right)p_{s+1,k}\right]w_m\Delta\Omega_m \\
& -\sum_{m=1}^{N_{gp}}\sum_{i=1}^{N_d}\left[\sum_{k=1}^{N_n}\frac{1}{6\mu_m}3h_m^2\left(\frac{\partial N_{mk}}{\partial x}p_{s,k}\frac{\partial W_{mj}}{\partial x}\right)C[j,i]_m p_{s+1,k}\right]w_m\Delta\Omega_m \\
& +U\sum_{m=1}^{N_{gp}}\sum_{i=1}^{N_d}\left[\sum_{k=1}^{N_n}W_{mj}\left(\frac{\partial N_{mk}}{\partial x}C[j,i]_m p_{s+1,k}\right)\right]w_m\Delta\Omega_m \\
& +\frac{2}{\Delta t}\sum_{m=1}^{N_{gp}}\sum_{i=1}^{N_d}\left[\sum_{k=1}^{N_n}W_{mj}N_{mk}C[j,i]_m p_{s+1,k}\right]w_m\Delta\Omega_m \\
& +U\sum_{m=1}^{N_{gp}}\left[\sum_{k=1}^{N_n}W_{mj}\left(\frac{\partial N_{mk}}{\partial x}r_k h_k\right)\right]w_m\Delta\Omega_m \\
& +\frac{2}{\Delta t}\sum_{m=1}^{N_{gp}}\left[\sum_{k=1}^{N_n}W_{mj}N_{mk}\left(r_k\left(t\right)h_k\left(t\right)-r_k\left(t-\Delta t\right)h_k\left(t-\Delta t\right)\right)\right]w_m\Delta\Omega_m \\
& -\sum_{m=1}^{N_{gp}}\sum_{i=1}^{N_d}\left[\sum_{k=1}^{N_n}\frac{1}{6\mu_m}3h_m^2\left(\frac{\partial N_{mk}}{\partial x}p_{s,k}\frac{\partial W_{mj}}{\partial x}\right)C[j,i]_m p_{s,i}\right]w_m\Delta\Omega_m \\
& +U\sum_{m=1}^{N_{gp}}\sum_{i=1}^{N_d}\left[\sum_{k=1}^{N_n}W_{mj}\left(\frac{\partial N_{mk}}{\partial x}h_{g,m}\right)\right]w_m\Delta\Omega_m \\
& +\frac{2}{\Delta t}\sum_{m=1}^{N_{gp}}\sum_{i=1}^{N_d}\left[\sum_{k=1}^{N_n}W_{mj}N_{mk}C[j,i]_m p_{s,i}(t-\Delta t)\right]w_m\Delta\Omega_m \\
& -\frac{2}{\Delta t}\sum_{m=1}^{N_{gp}}\left[W_{mj}\left(h_m(t)-h_m(t-\Delta t)\right)\right]w_m\Delta\Omega_m = 0.
\end{aligned} \tag{3.29}$$

where the m-index defines a general Gauss point, w_m is the corresponding weight, $\Delta\Omega_m$ is the determinant of the coordinate transformation from the global coordinate system to the local element coordinate system, the k-index defines a general element node and N_{gp}, N_n and N_d represent the number of Gauss points, the number of nodes for each element and the total number of nodes in the domain, respectively.

Writing Eqn.(3.29) for each node of the domain, a system of non-linear algebraic equations is obtained, the variables being p_{s+1} and r. The system is in the form of Eqn.(2.44):

$$[A]\,p + [B]\,r + C = 0, \tag{3.30}$$

where:

$$\begin{aligned}
A_{j,k} = \sum_{n=1}^{N_e} \Bigg\{ & - \sum_{m=1}^{N_{gp}} \left[\sum_{k=1}^{N_n} \frac{1}{6\mu_m} h_m^3 \left(\frac{\partial N_{mk}}{\partial x} \frac{\partial W_{mj}}{\partial x} \right) \right] w_m \Delta\Omega_m \\
& - \sum_{m=1}^{N_{gp}} \sum_{i=1}^{N_d} \left[\sum_{k=1}^{N_n} \frac{1}{6\mu_m} 3h_m^2 \left(\frac{\partial N_{mk}}{\partial x} p_{s,k} \frac{\partial W_{mj}}{\partial x} \right) C[j,i]_m \right] w_m \Delta\Omega_m \\
& + U \sum_{m=1}^{N_{gp}} \sum_{i=1}^{N_d} \left[\sum_{k=1}^{N_n} W_{mj} \left(\frac{\partial N_{mk}}{\partial x} C[j,i]_m \right) \right] w_m \Delta\Omega_m \\
& + \frac{2}{\Delta t} \sum_{m=1}^{N_{gp}} \sum_{i=1}^{N_d} \left[\sum_{k=1}^{N_n} W_{mj} N_{mk} C[j,i]_m \right] w_m \Delta\Omega_m \Bigg\}
\end{aligned} \tag{3.31}$$

$$\begin{aligned}
B_{j,k} = \sum_{n=1}^{N_e} \Bigg\{ & + U \sum_{m=1}^{N_{gp}} \left[\sum_{k=1}^{N_n} W_{mj} \left(\frac{\partial N_{mk}}{\partial x} h_k \right) \right] w_m \Delta\Omega_m \\
& + \frac{2}{\Delta t} \sum_{m=1}^{N_{gp}} \left[\sum_{k=1}^{N_n} W_{mj} N_{mk} h_k(t) \right] w_m \Delta\Omega_m \Bigg\}
\end{aligned} \tag{3.32}$$

$$\begin{aligned}
C_j = \sum_{n=1}^{N_e} \Bigg\{ & - \sum_{m=1}^{N_{gp}} \sum_{i=1}^{N_d} \left[\sum_{k=1}^{N_n} \frac{1}{6\mu_m} 3h_m^2 \left(\frac{\partial N_{mk}}{\partial x} p_{s,k} \frac{\partial W_{mj}}{\partial x} \right) C[j,i]_m p_{s,i} \right] w_m \Delta\Omega_m \\
& + U \sum_{m=1}^{N_{gp}} \sum_{i=1}^{N_d} \left[\sum_{k=1}^{N_n} W_{mj} \left(\frac{\partial N_{mk}}{\partial x} h_{g,m} \right) \right] w_m \Delta\Omega_m \\
& + \frac{2}{\Delta t} \sum_{m=1}^{N_{gp}} \sum_{i=1}^{N_d} \left[\sum_{k=1}^{N_n} W_{mj} N_{mk} C[j,i]_m p_{s,i}(t - \Delta t) \right] w_m \Delta\Omega_m \\
& - \frac{2}{\Delta t} \sum_{m=1}^{N_{gp}} \left[W_{mj} \left(h_m(t) - h_m(t - \Delta t) \right) \right] w_m \Delta\Omega_m \\
& - \frac{2}{\Delta t} \sum_{m=1}^{N_{gp}} \left[\sum_{k=1}^{N_n} W_{mj} N_{mk} (r_k(t - \Delta t) h_k(t - \Delta t)) \right] w_m \Delta\Omega_m \Bigg\}
\end{aligned} \tag{3.33}$$

Chapter 4

Numerical Implementation

"Measure what is measurable, and make measurable what is not so."

Galileo Galilei

4.1 Test Cases

The examples covered in this section aim to compare the results obtained using the proposed formulation for compressible, piezoviscous and shear thinning fluids against other formulations and results reported in the literature and full CFD simulations.

4.1.1 Parabolic Slider

The first example case has been chosen to test the capabilities of the proposed algorithm versus other existing formulations of the Reynolds equation for compressible fluids [5, 6]. For this purpose, a test case similar to the one proposed by Sahlin et al. [6], which deals with a parabolic slider, has been analysed. In particular, the minimum and the maximum film thickness has been modified with respect to the original values adopted in [6] in order to emphasize the effect of compressibility. The compressible formulation employed is the Downson and Higginson equation with $C_1 = 2.22 \cdot 10^9$ and $C_2 = 1.66$. Piezoviscosity and shear thinning effects are not considered and excluded from the solver. Results are compared with those obtained with the algorithm proposed in [6], with the constant bulk modulus formulation proposed in [5] and with the incompressible case. The geometry of the slider is schematically described in Fig.4.1 . The parameters governing the problem are: bearing length, $a = 0.0762\,m$; $h_{min} = 4\,\mu m$; $h_{max} = 8\,\mu m$; $U = 4.57\,m/s$; $p_1 = 3.36414 \cdot 10^5\,Pa$; $p_2 = 0\,P_a$; $\beta = 6.9 \cdot 10^7\,Pa$; $\mu = 0.039\,Pa\,s$.

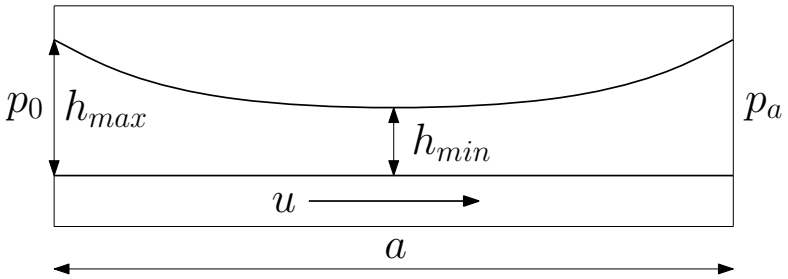

FIGURE 4.1: Schematic of the problem along with the description of the main symbol adopted

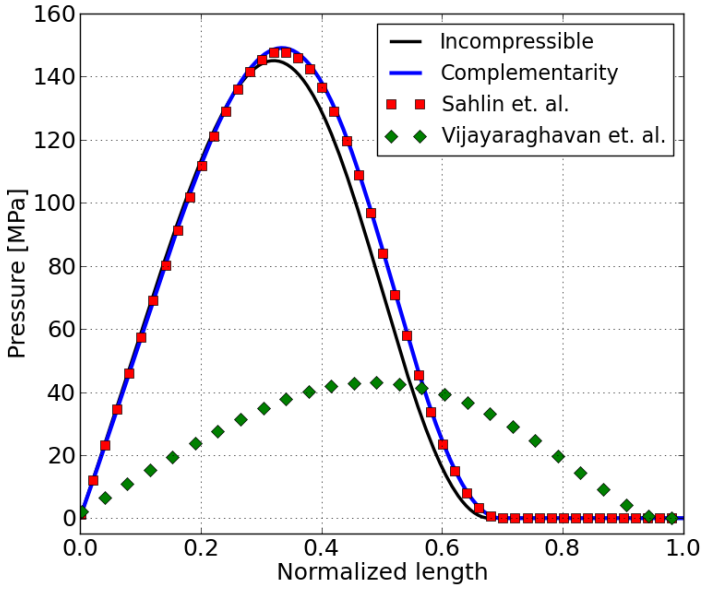

FIGURE 4.2: Pressure distribution for the different formulations considered

FIGURE 4.3: Comparison of the solutions obtained with different formulation for a single parabolic slider

A 300-elements discretization was employed. The system on which all the calculations have been performed is a single-core Intel Centrino @ 2.20 GHz. The time required for the numerical solution is approx 40 milliseconds.

Fig. 4.2 confirms the results obtained using the proposed algorithm are in good agreement with those obtained with the formulation by Sahlin et al. [6]. A $\approx 0.7\%$ difference in peak pressure between the proposed formulation and the one presented in [6] has been detected and the boundaries separating the active and the cavitated regions coincide. Fig. 4.2 also highlights the limitations of the constant bulk modulus compressibility formulation in the case of high values of pressure. The curve that corresponds to the formulation proposed in [5] differs noticeably from the others.

To asses the capability of the proposed algorithm to correctly predict the fluid film reformation, another test case proposed by Sahlin et al. [6] is presented, which deals with

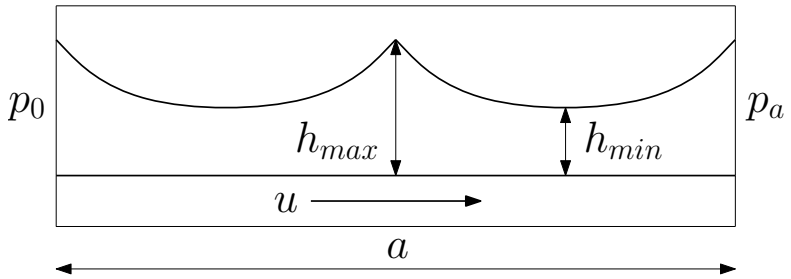

FIGURE 4.4: Schematic of a twin parabolic slider

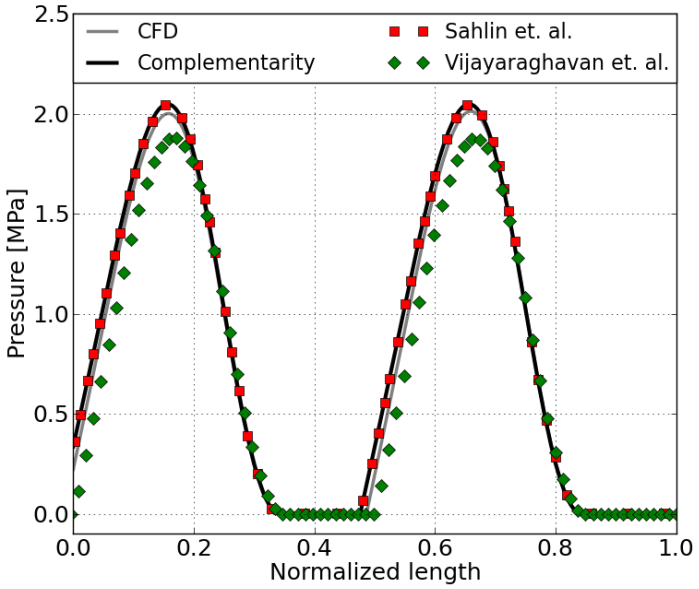

FIGURE 4.5: Pressure solutions for the different formulations considered

FIGURE 4.6: Comparison of the solutions obtained with different formulation for a single parabolic slider

a twin parabolic slider. A schematic representation of the problem under investigation is reported in Fig. 4.4 and the main geometrical and physical parameters are the same as those used for the previous example problem. The results obtained with the proposed algorithm are compared with both a full CFD analysis based on the complete Navier-Stokes equations performed using OpenFOAM and, again, with the methods developed in [5] and [6]. The cavitation model used in the CFD package is the Isobaric Cavitation Model (ICM), which has been implemented and tested in [33, 34]. The domain has been discretized with 400 elements and the calculation time is slightly less than 100 milliseconds. Fig. 4.5 shows the comparison of the pressure distributions obtained with the different formulation considered.

Again, a very good agreement has been found between the present formulation and the one proposed by Sahlin et al. (peak pressure difference $\leq 0.1\%$) and with the

OpenFoam CFD simulation (peak pressure difference $\leq 0.7\%$ [1]). Also the location of rupture and reformation boundaries are similarly detected by the three formulations mentioned above. On the other hand, the constant bulk modulus formulation again underestimates the peak pressure and fails to locate the correct reformation boundary.

4.1.2 Journal bearing with piezoviscous lubricant

The problems analyzed in this section aim to validate the piezoviscosity method adopted. In particular, two different test configurations are taken from the work of Gwynllyw et at. [24], where the flow of an incompressible piezoviscous lubricant in a journal bearing is considered.

The calculations performed refer to the configurations showed in Fig. 14 and Fig. 15 of [24]. The main parameters of the problem follow: the radii of the journal and of the bearing are, namely, $r_j = 31.25\,mm$ and $r_b = 31.29\,mm$, the angular velocity is $\omega = 250\,rad/s$ and the viscosity at ambient pressure is $\mu_0 = 5.7\,mPa\,s$. The radial clearance is $c = r_b - r_j = 0.04\,mm$, the distance between the center of the journal and the bearing is labelled as e, while the ratio e/c is named eccentricity ratio. In particular, two different configurations defined by $e/c = 0.93$ and $e/c = 0.95$ are investigated.

The Barus model for piezoviscosity is employed with a piezoviscous coefficient $\alpha = 1.12 \cdot 10^{-8}\,/Pa$. The cavitation model used by [24] handles the cavitation by decreasing the viscosity in the regions where the pressure gets values lower than the cavitation pressure. This cavitation model does not provide a zero-gradient pressure at the onset of cavitation, which is, instead, correctly predicted by the formulation favoured in this work, resulting in a slightly different upstream pressure. In order to assess the accuracy of the piezoviscous model implemented in the proposed algorithm, the author deemed essential to compare formulations that predict same solutions for isoviscous fluids. Therefore, for these test cases only, the same cavitation model employed in [24] has been implemented in place of the complementarity approach. This has been achieved by setting the cavitation pressure in the algorithm low enough so cavitation does not occur in the entire domain. Once the solution in terms of pressure is evaluated, the negative values of pressure are set to zero.

For these two simulation a 600-elements discretization has been employed and the time for the numerical solution is approx 0.2 seconds for the case of Fig. 4.7 and 1.5 seconds for the case of Fig. 4.8.

[1] The discrepancy with the CFD results is probably due to the inability to reproduce the exact boundary conditions at the inlet of the slider.

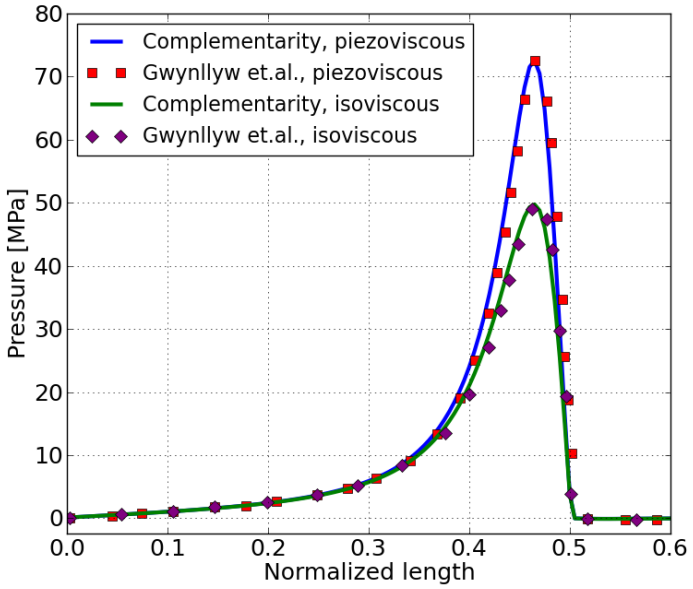

FIGURE 4.7: Comparison of the pressure solutions for isoviscous (dashed lines) and piezoviscous (solid lines) lubricants for a statically loaded journal for an eccentricity ratio $e/c = 0.93$

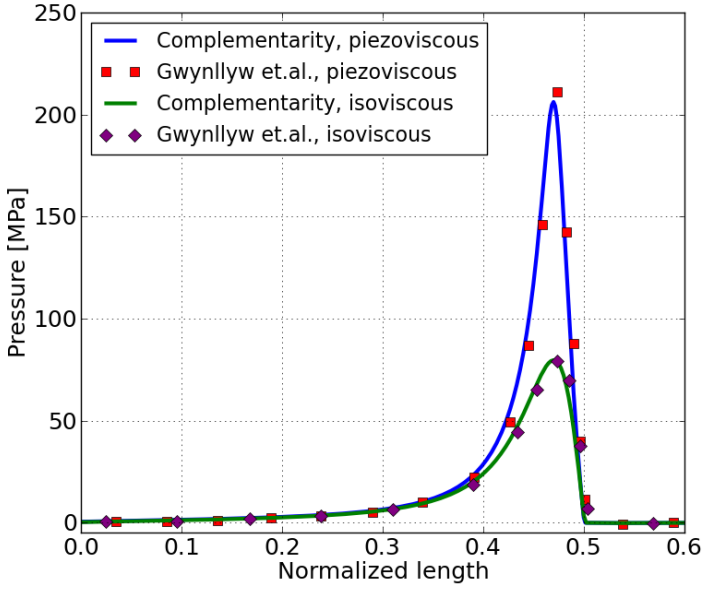

FIGURE 4.8: Comparison of the pressure solutions for isoviscous (dashed lines) and piezoviscous (solid lines) lubricants for a statically loaded journal for an eccentricity ratio $e/c = 0.95$

Fig. 4.7 and Fig. 4.8 show the pressure results for the two configuration analyzed. Both the isoviscous and the piezoviscous solution evaluated with the formulation favoured in this work match the ones reported in [24] with a peak pressure difference lower than 1.5%.

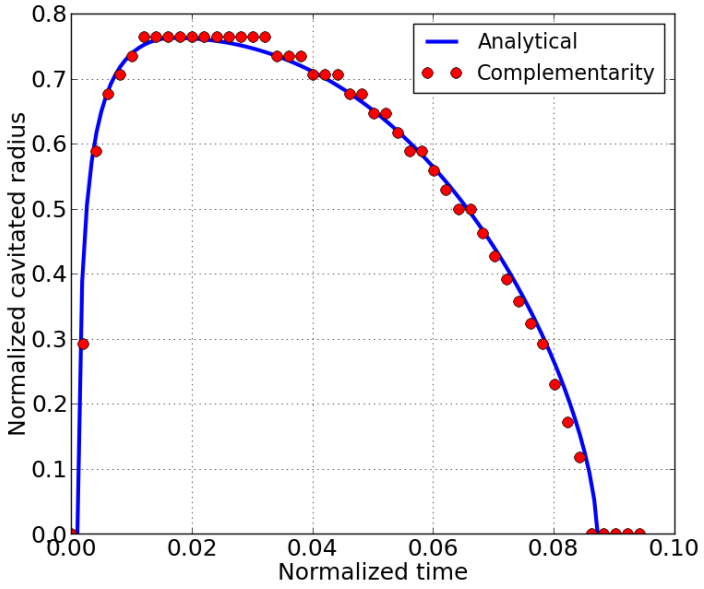

FIGURE 4.9: Extension of the cavitated zone in a pure squeeze motion for the proposed formulation and for the analytical solution.

4.1.3 Pure Squeeze

In the following, the extension to a two dimensional domain of the results reported in [10] for a pure squeeze motion is presented. The proposed formulation for two dimensional domains has been tested against an analytical model representing the extension of the one dimensional analytical model developed by Optasanu et al. in [35].

The problem deals with a thin film of liquid contained between two circular plates of finite radius. The two plates are moved apart and brought together following the sinusoidal law:

$$h(t) = h_{min} + h_a \left(1 - cos(\omega t)\right),$$

where the radius of the plates is $r_a = 5\,mm$, the minimum film thickness is $h_{min} = 9.14\,\mu m$, the half-amplitude of the axial displacement is $h_a = 320.8\,\mu m$, the viscosity is $\mu = 0.005\,Pa\,s$ and the speed is $\omega = 99.74\,rad/s$. For the numerical solution, a 3537-nodes domain has been employed and the simulation time has been divided in 96 steps. The time required for the calculation is approx 24 minutes. Fig. 4.9 depicts the variation in time of the extent of the cavitation zone for both the proposed complementarity formulation and for the analytical solution. The analytical solution for the two dimensional case is derived from [35] and it is detailed in appendix A.1

An excellent agreement is found between numerical and analytical results.

4.1.4 2D Pocket

The second two dimensional example deals with a micro-texture pocket considering a compressible, piezoviscous and shear-thinning fluid. Two different test configurations are analyzed: (i) the first test case is characterised by the following parameters (see Fig. 4.10): bearing size, $a = 20\,mm \times b = 10\,mm$; minimum and maximum film thickness,namely, $h_{min} = 1\,\mu m$ and $h_{max} = 1.1\,\mu m$; pocket depth $h_p = 0.4\,\mu m$; pocket width and length, $w = 7\,mm$ and $l = 6\,mm$; distance of the pocket from the inlet, $c = 4\,mm$; viscosity at ambient pressure, $\mu = 0.01\,Pa\,s$; cavitation pressure, $p_c = 0\,Pa$; pressure at the boundaries, $p_{amb} = 10^5\,Pa$; sliding speed, $U = 1\,m/s$; (ii) the second test case is characterised by the same parameters of test case (i) apart from the domain and pocket width, chosen to be thirty times wider ($b = 300\,mm$ and $w = 210\,mm$). The constant parameters C_1 and C_2 for the Dowson and Higginson equation are the same employed in the first example of this section. Piezoviscosity is modelled using the Barus's equation, Eqn.(2.6), with a piezoviscosity coefficient $\alpha = 1.2 \cdot 10^{-8}/Pa$ and the shear-thinning model is the Eyring sin-law equation, Eqn.(2.12), with $\tau_0 = 5\,MPa$. Both the simulations of case (i) and case(ii) have been performed with a domain composed of 3528 elements.

Fig. 4.11 and Fig. 4.12 depict the pressure and the normalized density ρ/ρ_c for the two dimensional pocket of case (i).

Fig. 4.14 compares the pressure profiles in the mid-section π of the two dimensional pocket of case (i) with the ones obtained with the JFO formulation by Ausas et. al. [1] and the two dimensional pocket of case (ii) with the one dimensional formulation by Giacopini et. al. [10].

This example shows how the two dimensional formulation derived in the present work correctly matches the results of previously validated formulations ([1, 10]). In fact, the difference in term of peak pressure between the favoured formulation and the corresponding curve in both case (i) and case (ii) is lower than 1%.

The extension to a two dimensional domain allows to evaluate bearing performances when more realistic, finite width, textures are considered.

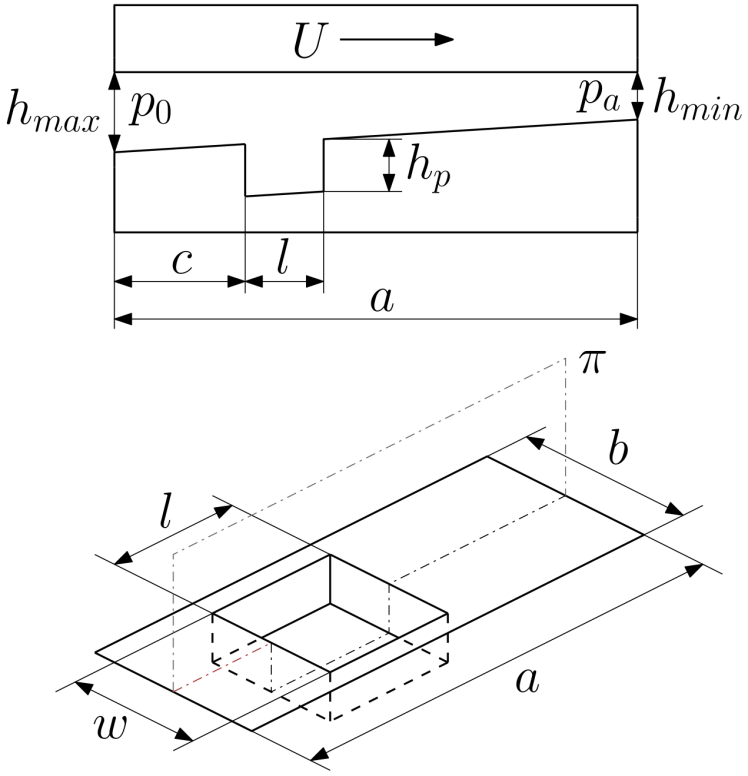

FIGURE 4.10: Schematic of a converging bearing containing a single micro-texture pocket, positioned toward the inlet, along with the description of the main symbol adopted (section π and isometric view)

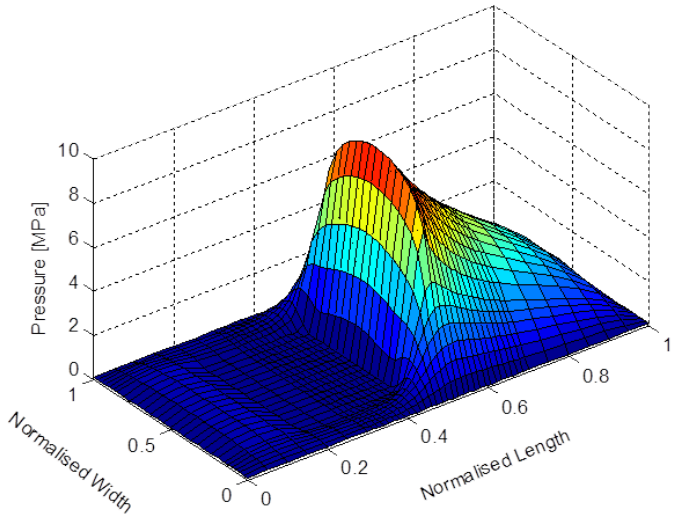

FIGURE 4.11: Waffle slipper-like pressure profile

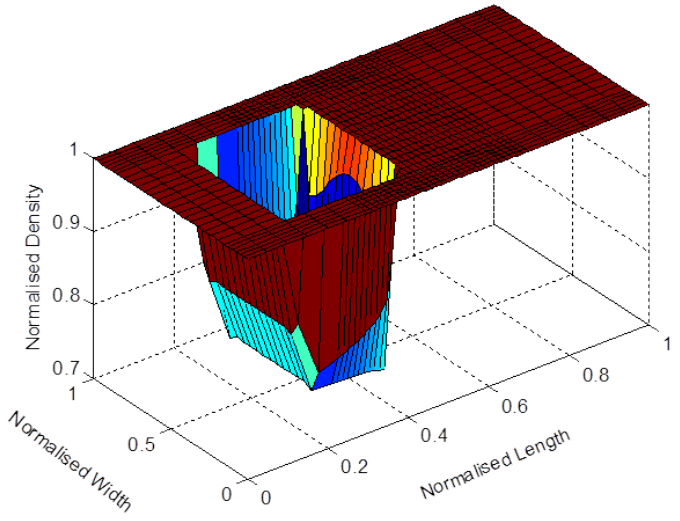

FIGURE 4.12: Normalized density

FIGURE 4.13: Pressure and normalized density for the two dimensional micro-texture pocket (i). The pocket width is $w = 7\,mm$.

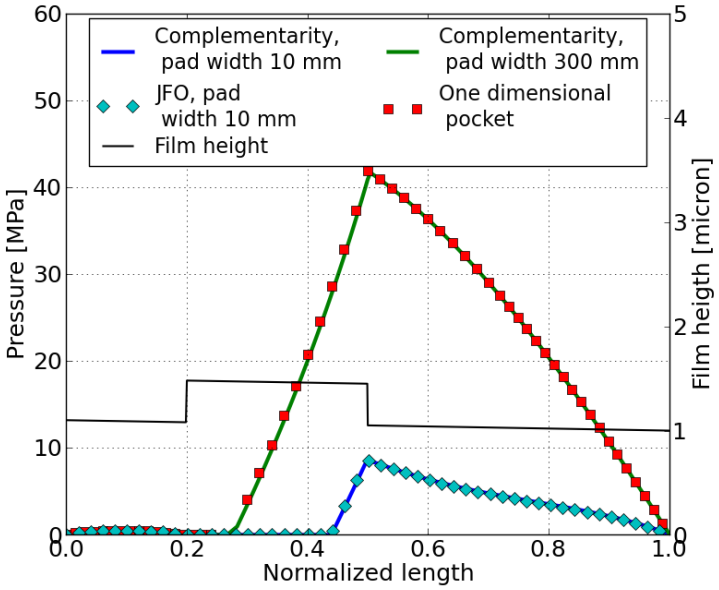

FIGURE 4.14: Comparison of the pressure profiles in the mid-section π. The complementarity solution for the pocket $10\,mm$ wide is compared with the JFO formulation provided in [1], and the complementarity solution for the pocket $300\,mm$ wide is compared with the one dimensional solution.

4.2 Journal Bearing

The example cases presented above are intended to prove the capabilities of the proposed formulation to solve a number of different problems, giving results that match with other formulations available in bibliography.

One application where EHL analysis have a great practical interest is the journal bearing lubrication analysis. The test case discussed in section (4.1.2) is a rigid one dimensional problem, where the film thickness is defined by the user. Lubrication analysis of real journal bearings require a different approach. As a start, the elastic deflection is not negligible as strongly affects the results in terms of pressure, void fraction and, especially, journal path. Moreover, when the axial length of the bearing in small compared to its radius, a two dimensional analysis is required and, finally, the approach where the film thickness is defined by the user has to be discharged for a more flexible and realistic implementation based on the equilibrium equation.

In fact, usually the loading history on the journal bearing is known and an important output of the analysis is the journal path and the minimum film thickness found.

For these reason, a more sophisticated and flexible numerical algorithm has been implemented, that solves at the same time the equilibrium and the EHL Reynolds equations. For each time step, the pressure and void fraction fields that solves the Reynolds equation are evaluated in all the nodes of the domains and the correct position of the journal centre is computed so that the resultant of pressure equals the external load in intensity and orientation with opposite direction.

The description of this implementation, along with a numerical example, follows.

4.2.1 Governing Equations

Reynolds equation for elastohydrodynamic lubrication The two dimensional Reynolds equation for compressible, piezoviscous and non-Newtonian fluids, recasted in terms of the functional derivative of p, suitable for the solution of EHL problem,

Eqn.(3.16), is here reported:

$$\begin{aligned}
&\frac{\partial}{\partial x}\left[f(p)\frac{h^3}{6\mu}\frac{\partial p}{\partial x}\right]\frac{\partial}{\partial y}\left[f(p)\frac{h^3}{6\mu}\frac{\partial p}{\partial y}\right] - 2\frac{\partial}{\partial t}\left[f(p)h\right] + 2\frac{\partial}{\partial t}\left[rh\right] \\
&\qquad -U\frac{\partial}{\partial x}\left[f(p)h\right] + U\frac{\partial}{\partial x}\left[rh\right] - U\frac{\partial}{\partial y}\left[f(p)h\right] + U\frac{\partial}{\partial y}\left[rh\right] = 0 \\
&\qquad\qquad h = h_g + \ell p \\
&\qquad\qquad p \geq 0 \\
&\qquad\qquad r \geq 0 \\
&\qquad\qquad p \cdot r = 0.
\end{aligned} \tag{4.1}$$

Equilibrium equation It is possible to consider the bearing fixed and the loads applied to the journal (the following discussion and equations are valid also in the case of a fixed journal, where the loads are applied to the bearing). In this case, the equilibrium equations in cylindrical coordinates are:

$$\begin{cases} \int_\Omega p(\theta, z)\cos(\theta)d\Omega = F_x(t) \\ \int_\Omega p(\theta, z)\sin(\theta)d\Omega = F_y(t) \end{cases} \tag{4.2}$$

The calculation of the forces acting on the journal bearing is based on the geometrical properties, the mass properties and working conditions of the connecting rod assembly.

The schematic of Fig.4.15 shows the assembly along the most important dimension. For the particular case considered, the external force has been evaluated with a complex simulation of the engine dynamics, which discussion is out of the scope of the topic of this thesis. The interest reader is referred to specialized sources on the dynamic of system with high number of degree of freedom.

Oil supply hole The crankshaft pin presents a hole to supply lubricant to the journal bearing. The oil supply tank is pressurized, and the pressure of the oil at the inlet hole is given by the sum of the tank pressure and the centrifugal contribution, labelled by the subscript ω, due to the rotation of the crankshaft (see Fig.4.16).

$$p_{inlet} = p_{supply} + p_\omega \tag{4.3}$$

where

$$p_{h,\omega} = |\bar{r}_c + \bar{r}_{ph}|\omega. \tag{4.4}$$

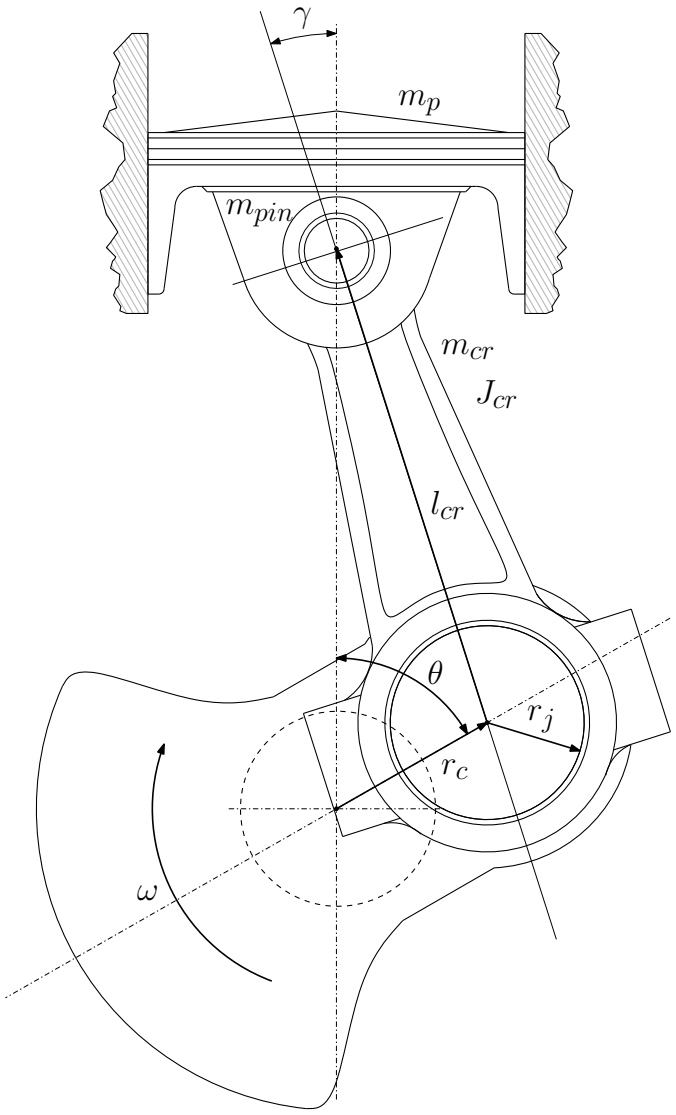

FIGURE 4.15: Schematic of the connecting rod assembly along with the most important dimensions, angles, geometrical and mass property

Lubricant model The lubricant is compressible, following the Dowson and Higginson equation (Eqn.(2.4)). The piezoviscosity is modelled with the Rodermund equation, see Eqn.(2.11) and the shear thinning behaviour is evaluated with Eqn.(2.13).

The value of the various coefficients is given in Table 4.3.

The influence of the temperature on the lubricant properties is not considered because the analysis is isothermal, the temperature of the lubricant being $T = 100C$.

Elastic deflection The compliance matrix of the structure has been extracted from a finite element model of the connecting rod and crank pin. The values of the Young's modulus and of the Poisson ratio are defined in Table 4.1.

Fig.4.17 shows the mesh of the connecting rod. The mesh of the Finite Element structural model has been converted and reduced to match the EHL domain employed for the lubrication analysis. The discretization parameters are detailed in Table 4.4.

4.2.2 Numerical Algorithm

"Turing Test Extra Credit: Convince the examiner that he's a computer."

Randall Munroe, xkcd webcomic

The simultaneous solution of the set of equation of Eqn. (4.1) and Eqn.(4.2) gives the journal position, $\bar{e}$, at each time step of the simulation.

To achieve this, two nested iterative loops have been implemented: the inner loop solves the EHL Reynolds equation in the pressure and void fraction variables given the journal position, the outer loop finds the correct journal position to match the external load[2]. This procedure is executed for every time step.

The pseudocode of this procedure if reported in Algorithm 1.

```
Initialization;
for t ← t_0 to t_f do
    F_x = F_x(t);
    F_y = F_y(t);
    while W_x ≠ F_x ∧ W_y ≠ F_y do
        J ← [dW̄/dē];
        guess a new journal position;
        ē ← ē − (W̄ − F̄) · [J]^{-1};
        h_g ← update geometric thickness;
        while convergence of p ∧ r ∧ h_e do
            update lubricant properties;
            h_e = [C] · p_s;
            p, r ← EHL Reynolds equation solution;
        end
        W_x ← ∫_Ω p(θ, z) cos(θ) dΩ;
        W_y ← ∫_Ω p(θ, z) sin(θ) dΩ;
    end
end
```

Algorithm 1: Pseudocode of the solving procedure.

The convergence of the solution of the inner loop is favourite (but not guaranteed) by the Newton method procedure used to solve the EHL Reynolds equation.

[2]There are very few problems that can't be solved with a well-placed goto instruction...

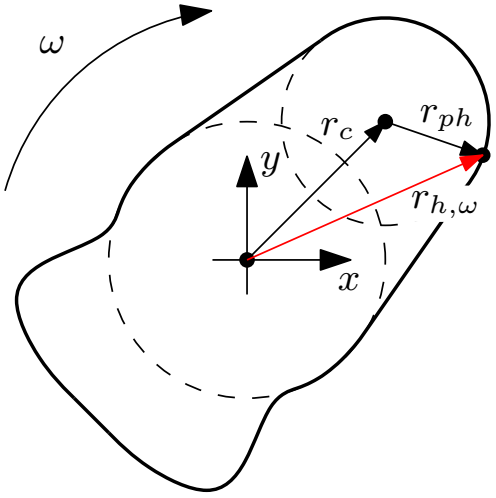

FIGURE 4.16: Crankshaft section. The position of the oil supply hole is highlighted and the meaning of the main symbols are depicted

FIGURE 4.17: Mesh of the connecting rod

The procedure employed for the outer loop is also a Newton method, that allows a quick convergence and saves computational time. In fact, the benefits of the quadratic convergence overcome the cost of the evaluation of the Jacobian [3].

In the case that the hydrodynamic effect is not sufficient to sustain the external load, dry contact may occur between the journal and the bearing and the lubrication regime switch from hydrodynamic to mixed. To handle this phenomenon, the linear complementarity formulation for mixed lubrication, explained in Section 5.2, is coupled with the EHL formulation proposed in this thesis.

The developed numerical procedure is stable and robust in the cases where the lubrication regime is hydrodynamic.

4.2.3 Results and Discussion

The main geometrical parameters of the journal bearing are presented in Table 4.1 while the physical properties of the lubricant are listed in Table 4.3. The analysis of performed considering the engine at full speed, 17500 rpm, and full power. The boundary conditions of the simulation are presented in Table 4.2 and the most important numerical setting are showed in Table 4.4. The connecting rod big end is not circular but, instead, presents a lemon shape. The radial clearance in the direction of the axis of the connecting rod is different than the one in the transversal direction. It presents also two dams in correspondence of the connection between the connecting rod and the cap.

The loads acting on the journal, F_x and F_y, are showed in Fig.4.18 and the relative coordinate system is discussed in Fig.4.16. Fig.4.19 depicts the load diagram. The

[3] In one dimension the numerical calculation of the Jacobian requires two solution of the EHL Reynolds equation, for a two dimensional domain it requires four solution

Journal Bearing data			
Property	Symbol	Value	Unit
Journal radius	r	20	mm
Bearing axial length	b	18	mm
Radial clearance (axial direction)	c	0.03	mm
Radial clearance (transversal direction)	c_t	0.07	mm
Dam depth	d	0.02	mm
Supply hole angle	θ_s	60	deg
Supply hole radius	r_s	1.2	mm
Young's Modulus	E	110000	MPa
Poisson Ratio	nu	0.3	-

TABLE 4.1: Journal data

transversal force, F_y, is caused principally by the inertial force and, therefore, follows a sinusoidal trend. The force directed as the connecting rod axis, F_x, is caused by the inertial force and the gas pressure. It mainly follows a sinusoidal trend shifted a quarter of cycle to the left with respect to F_y, the amplitude being higher. At time $t = 0$ the piston is at the top dead centre of the combustion stroke and the x component of the force due to the gas pressure overcome the inertial force.

Boundary conditions			
Property	Symbol	Value	Unit
Ambient pressure	p_{amb}	0.09	MPa
Cavitation pressure	p_{cav}	0.0	MPa
Oil supply pressure	p_{supply}	1.0	MPa
Crank radius	r_c	21.5	mm
Engine angular speed	ω	1833	rad/s

TABLE 4.2: Boundary conditions at 17500 rpm

Lubricant physical data			
Property	Symbol	Value	Unit
Base viscosity	μ_0	0.011	Pa s
Rodermund coeff	a_r	0.0028	Pa^{-1}
	b_r	2.8	-
Compressibility coeff.	$C1$	0.59e+3	MPa
	$C2$	1.34	-
Oil density	ρ	820	kg/m^3

TABLE 4.3: Lubricant data

Numerical Settings		
Mesh size	97x14	
Time step	361	
Nodes per element	4	
Simulation Time	0.020	s
Load capacity convergence test	1.0	N
Viscosity convergence test	$\mu_0 \cdot 10^{-2}$	Pa s
Deflection convergence test	10^{-7}	mm
Pressure residual test	$p_{amb} \cdot 10^{-2}$	MPa
Pressure relaxation	1.0	
Void fraction relaxation	1.0	
Elastic deflection relaxation	1.0	
Viscosity relaxation	0.25	
Jacobian dx	$10^{-6}\lvert c - \bar{e}\rvert$	mm

TABLE 4.4: Numerical settings chosen to simulate four cycles

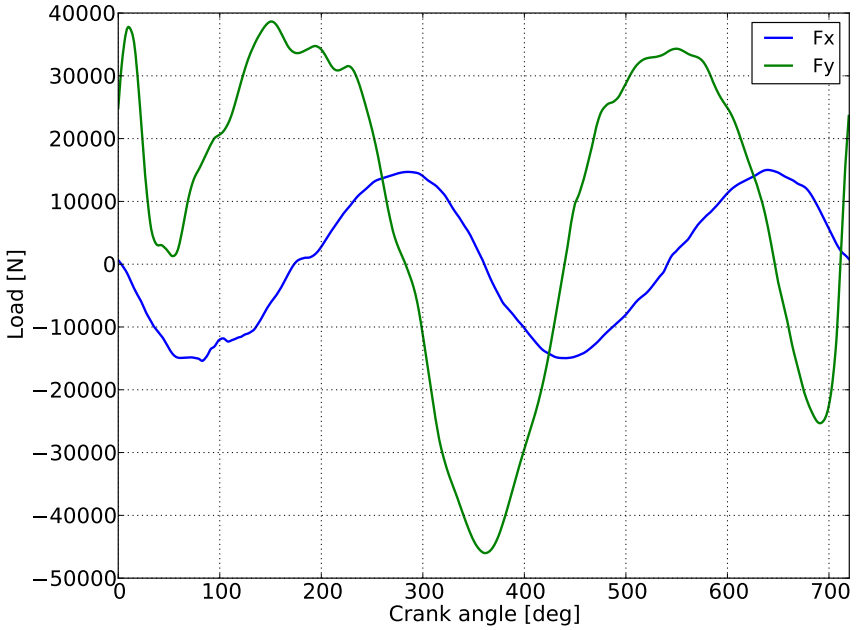

FIGURE 4.18: External load for the connecting-rod bearing

The lubricant is compressible, piezoviscous and shear thinning and the solid surfaces are elastic. Two different cases have been analysed:

1. No oil supply hole
2. With oil supply hole, which parameters defined in Tables 4.1 and 4.2

Fig.4.20 shows the comparison of the orbit diagrams for the two cases analysed. It is possible to note influence of the oil supply hole, that increase the load capacity in the critical instant of the combustion. The maximum eccentricity of the journal centre is 78.6μm and is found in the case without oil supply hole, while in the other two cases the maximum eccentricity is 78.3μm.

Fig.4.21 compares the minimum film thickness versus the crank angle for the two configuration analysed. The curves show qualitatively the same trend: the film thickness is maximum in the transient during the combustion and is minimum (dry contact occurs) at the top dead centre at the beginning of the intake stroke and during the compression stroke. It is evident that the oil supply increases the film thickness and reduces the dry contacts.

It is possible also to calculate the instantaneous flow rate and the total amount of oil. Fig.4.22 show the instantaneous mass of oil in the bearing as a function of the crank angle.

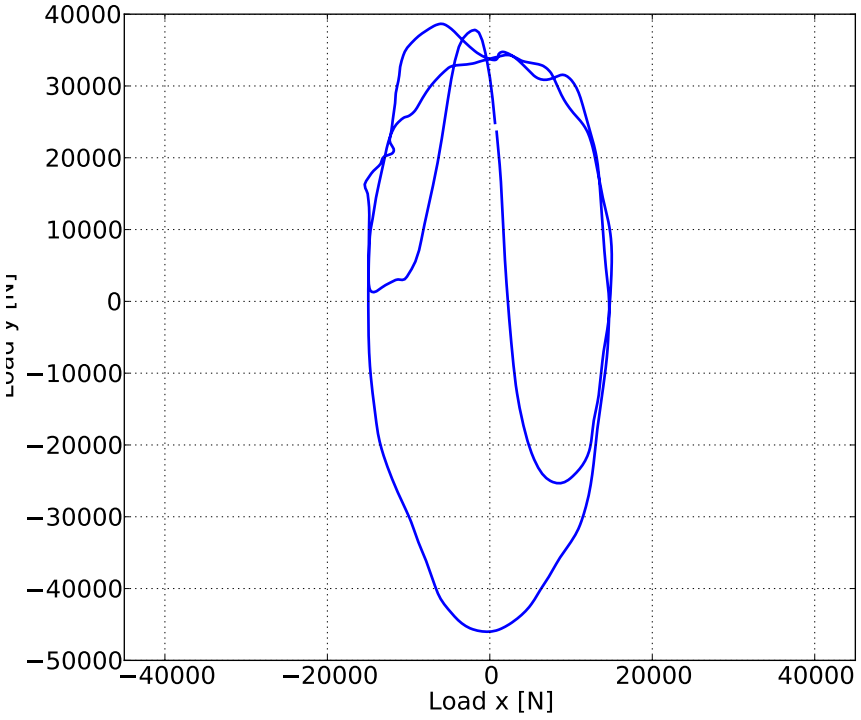

FIGURE 4.19: Load diagram for a connecting-rod bearing

The mass of oil present in the lubricating film can be calculated by integration of the density over the volume.

$$m_{oil} = \int_V \rho d\Omega \tag{4.5}$$

where V is the volume of lubricant. Substituting Eqn.(2.14) in Eqn.(4.5), and considering that the Reynolds equation assumes the fluid properties constant along the thickness:

$$m_{oil} = \int_A (1-r)\rho_c f(p) d\Omega. \tag{4.6}$$

The instantaneous flow rate is evaluated by derivation of the mass with respect to time:

$$\dot{m}_{oil} = \frac{\partial}{\partial t} \int_A (1-r)\rho_c f(p) d\Omega. \tag{4.7}$$

Fig.4.22 compares the lubricant mass versus the crank angle for the two cases analysed. It is evident that the presence of the oil supply hole increase the total amount of mass and. The maximum amount of lubricant mass for both cases is found at the top dead centre at the beginning of the intake stroke, whereas the lowest values are found during the combustion stroke. The high squeeze in correspondence of the combustion cause a sudden drop the oil mass.

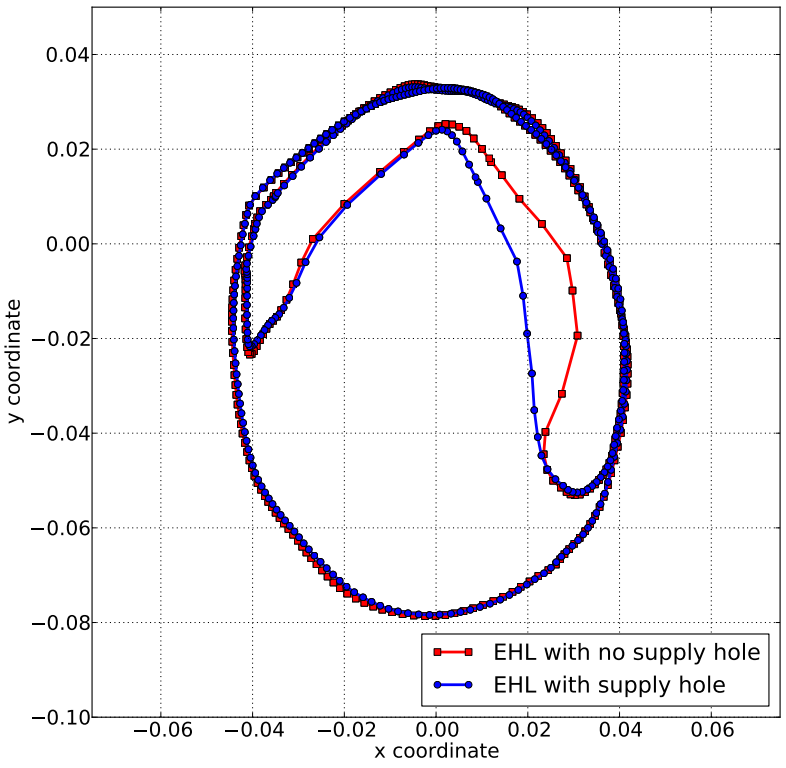

FIGURE 4.20: Comparison of the orbit diagrams for the journal bearing with and without the oil supply hole. Solid surfaces are elastic and the lubricant is compressible, piezoviscous and shear thinning.

Fig.4.23 and Fig.4.24 depict the mass variation of oil and the oil flux across the boundaries.

The integral on the cycle of the oil flux across the boundary is zero because the bearing is working at a steady state condition.

In the case of bearing without the oil supply hole the two curves coincide (the little differences are ascribable to the discretization process and to the numerical calculation of the flux, performed with a first order finite difference scheme). On the other hand, in the presence of the oil supply inlet, the mean flux across the side boundary of the bearing is lower than zero (outflow of the oil) while across the boundary of the oil inlet the mean flow is positive (the oil enter in the bearing). The sum of the two values (side and inlet) is obviously zero. The mass of oil that flows out the bearing each cycle is 6.59 g.

Fig.4.25 and Fig.4.26 show the mass flux across the side boundary as a function of the position (x axis) and versus the crank angle. It is possible to note in both cases the outflow in correspondence of the combustion and of the two side dams.

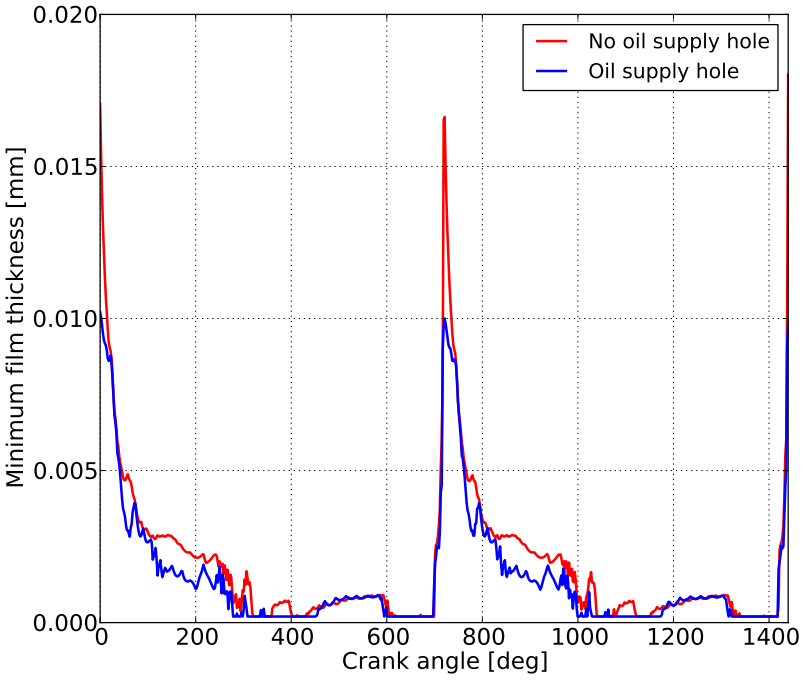

FIGURE 4.21: Minimum film thickness for the three cases analysed.

In the following, various plot are presented for the EHL journal bearing analysis. Each group of figures refers to different instants of the engine cycle:

- Fig.4.31: crank angle = 0 degree
- Fig.4.36: crank angle = 180 degree
- Fig.4.41: crank angle = 360 degree
- Fig.4.46: crank angle = 540 degree

Because of the symmetry of the problem with respect to the plane identified by the axis of the connecting rod in its cyclic motion, only half of the bearing has been modelled and symmetry boundary conditions have been imposed.

In Fig.4.31, which correspond to the combustion phase, the squeeze effect is prevalent and the pressure distribution is approximately symmetric with respect to the middle plane of the bearing. Moreover, this effect prevents dry contact between the journal and the bearing.

Fig.4.36 and Fig.4.46 show similar pressure and void fraction distribution. In fact the external load is similar in these two different instant.

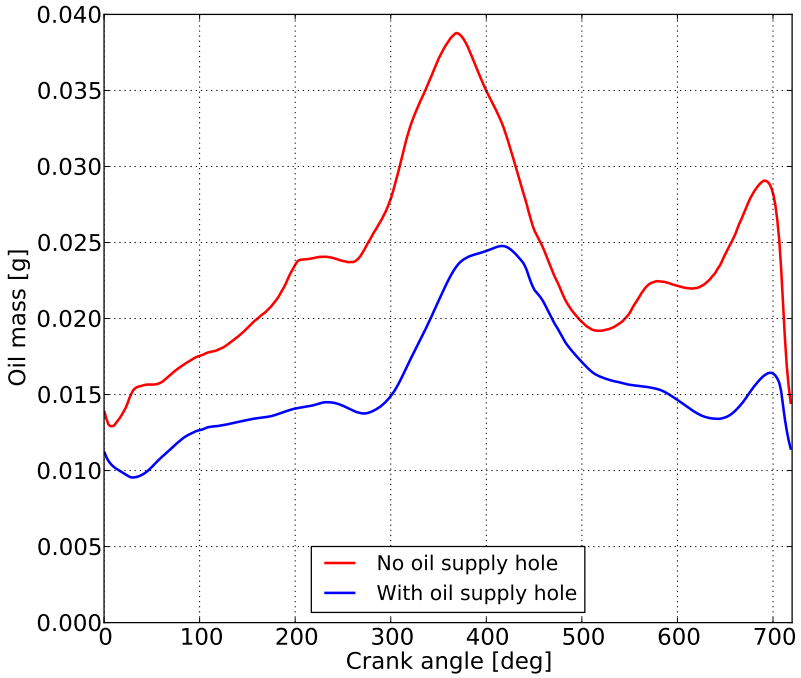

FIGURE 4.22: Instant total mass of oil present in the lubricant film with and without the oil supply hole.

Fig.4.41 freeze the moment where the connecting rod is under a traction load. The pressure peak is oriented in the direction of the connecting rod cap.

Fig.4.51 shows the film thickness all over the bearing in four different crank angle positions. The two plots which represent the thickness at the bottom dead centre show similar values. The thickness distribution in Fig.4.47 derives from the great influence of the squeeze effect during the combustion. In Fig.4.50 the thickness is minimum in the middle of the cap, unlike the other three distributions where the minimum is found on the opposite side.

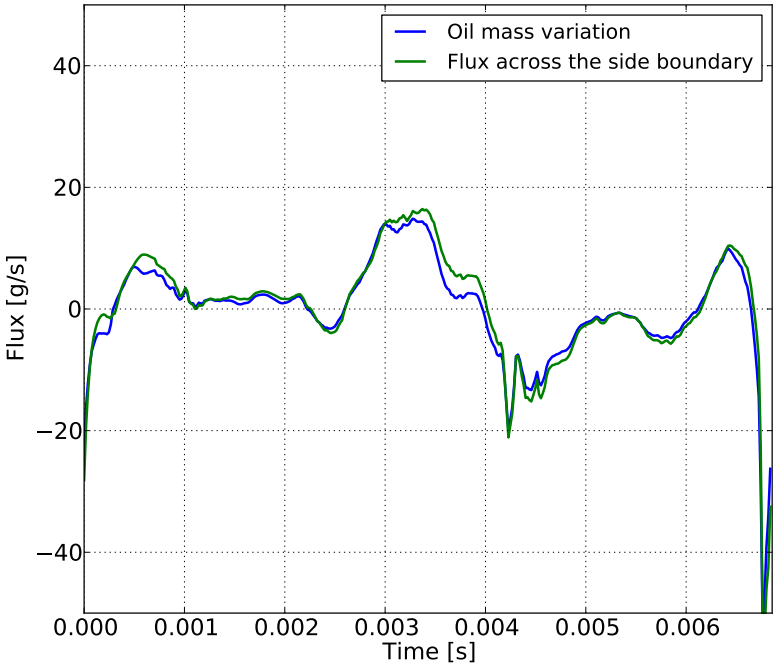

FIGURE 4.23: Oil mass variation and total flow rate across the side boundary for the configuration without supply hole.

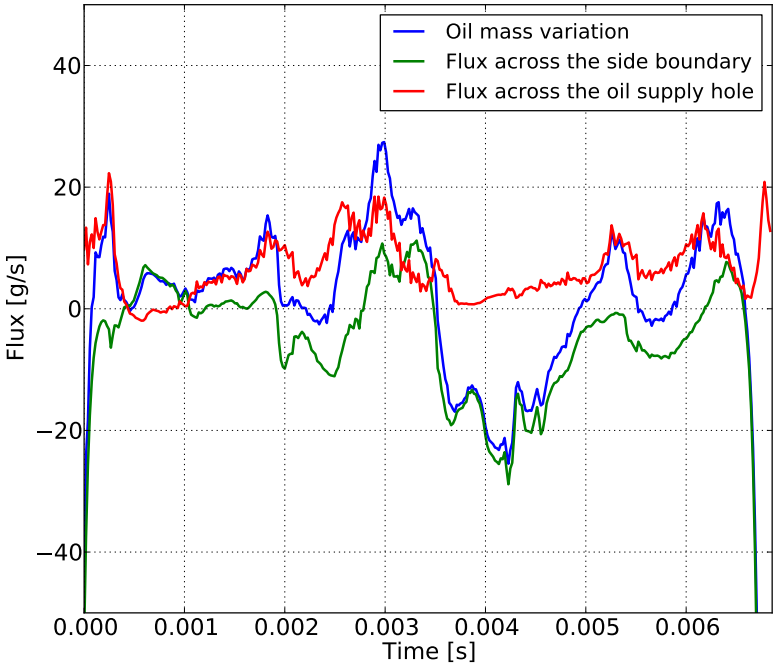

FIGURE 4.24: Oil mass variation, oil flow rate across the boundaries for the configuration with the oil supply hole.

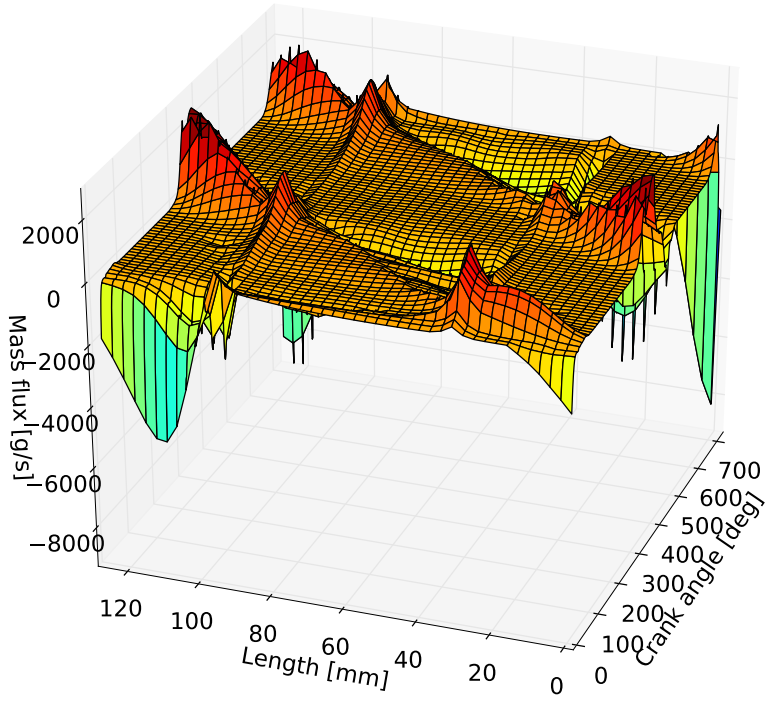

FIGURE 4.25: Mass flux across the side boundary length during a complete engine cycle for the configuration without the oil supply hole.

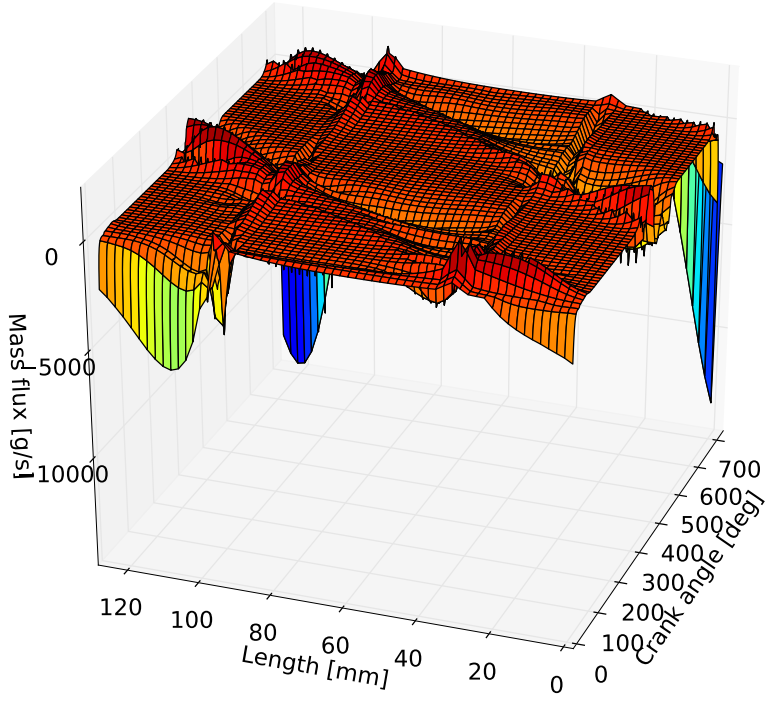

FIGURE 4.26: Mass flux across the side boundary length during a complete engine cycle for the configuration with the oil supply hole

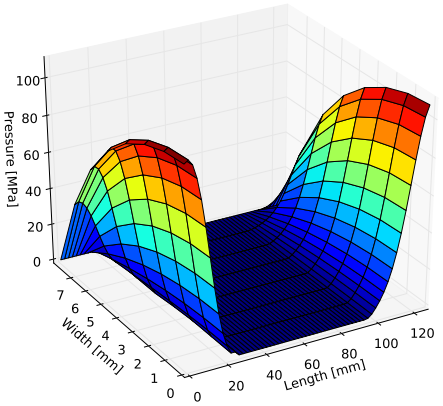

FIGURE 4.27: Hydrodynamic pressure

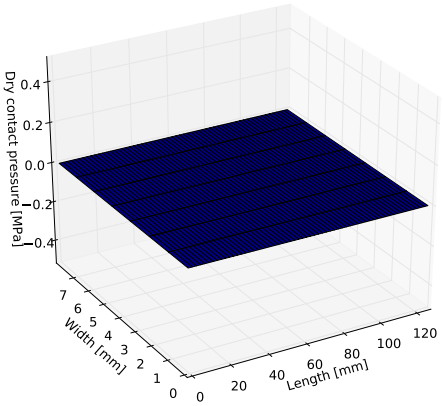

FIGURE 4.28: Dry contact pressure

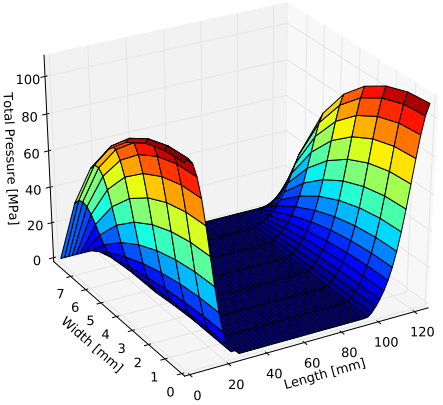

FIGURE 4.29: Total pressure

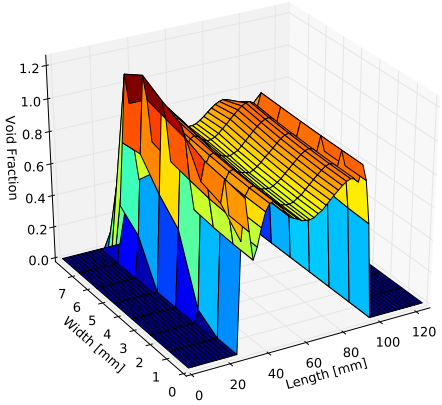

FIGURE 4.30: Void fraction

FIGURE 4.31: Various plot regarding the EHL journal bearing analysis in the presence of the oil supply hole at a crank angle $\theta = 0$, which corresponds to the Top Dead Centre at the beginning of the power stroke. Note that no dry contact is detected.

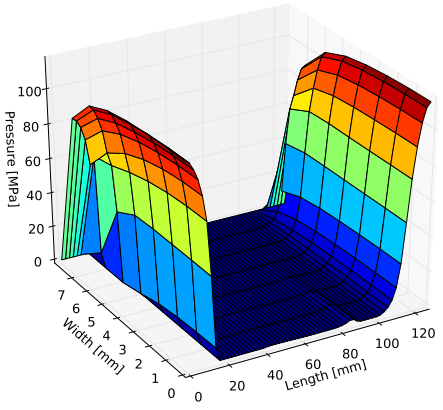

FIGURE 4.32: Hydrodynamic pressure

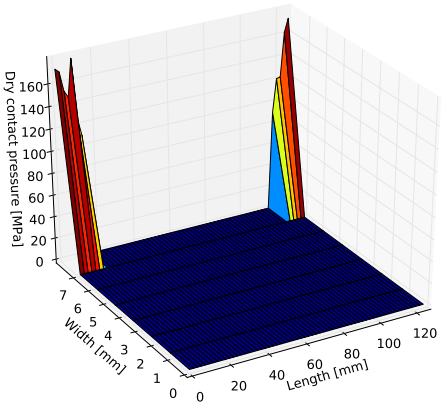

FIGURE 4.33: Dry contact pressure

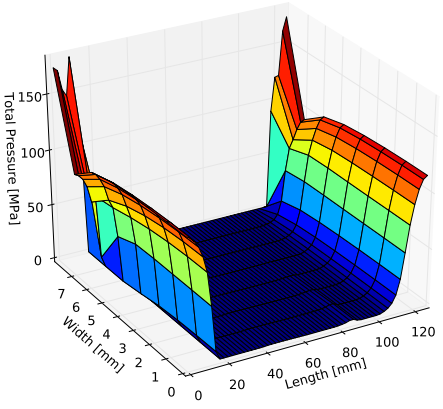

FIGURE 4.34: Total pressure

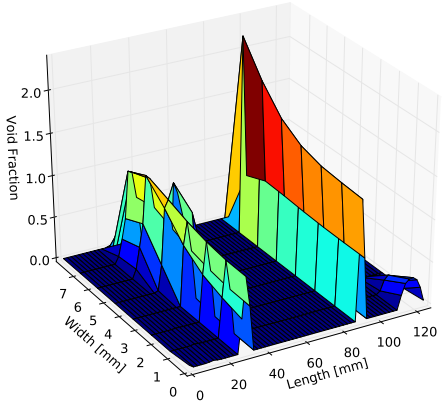

FIGURE 4.35: Void fraction

FIGURE 4.36: Various plot regarding the EHL journal bearing analysis in the presence of the oil supply hole at a crank angle $\theta = 180$, which corresponds to the Bottom Dead Centre at the end of the power stroke.

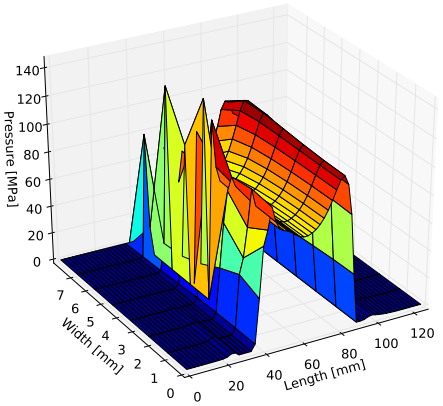

FIGURE 4.37: Hydrodynamic pressure

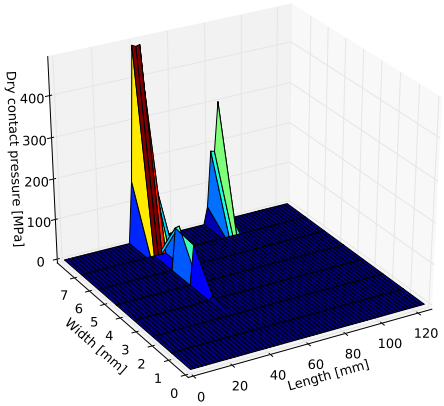

FIGURE 4.38: Dry contact pressure

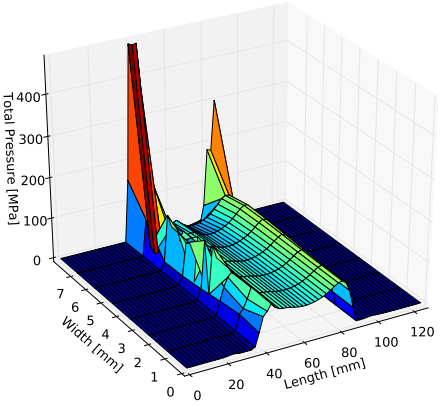

FIGURE 4.39: Total pressure

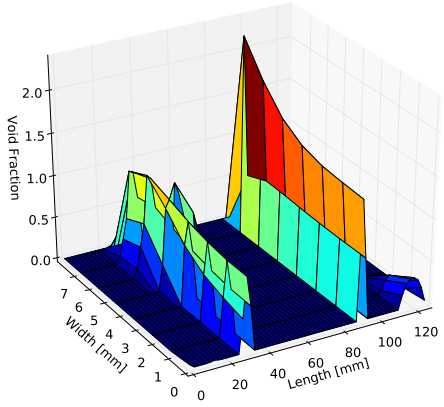

FIGURE 4.40: Void fraction

FIGURE 4.41: Various plot regarding the EHL journal bearing analysis in the presence of the oil supply hole at a crank angle $\theta = 360$, which corresponds to the Top Dead Centre at the beginning of the intake stroke

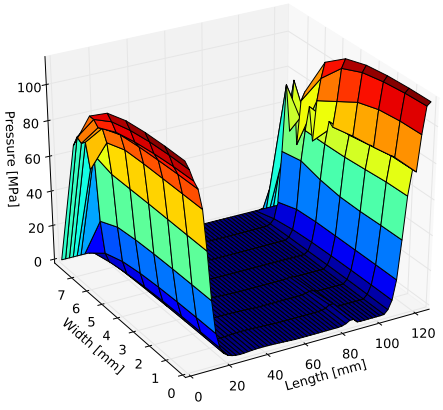

FIGURE 4.42: Hydrodynamic pressure

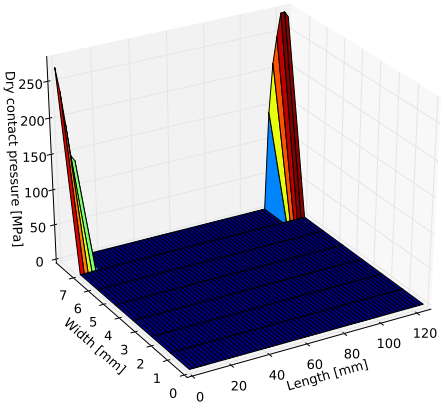

FIGURE 4.43: Dry contact pressure

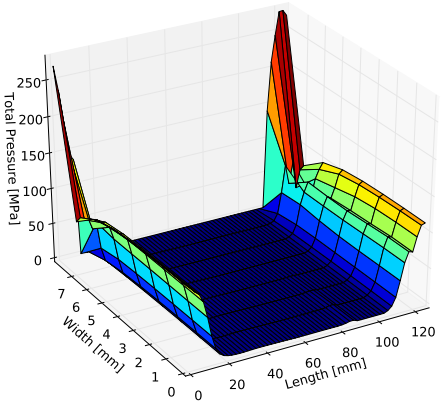

FIGURE 4.44: Total pressure

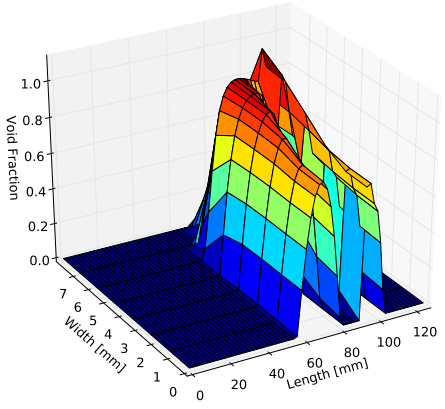

FIGURE 4.45: Void fraction

FIGURE 4.46: Various plot regarding the EHL journal bearing analysis in the presence of the oil supply hole at a crank angle $\theta = 540$, which corresponds to the Bottom Dead Centre at the beginning of the compression stroke

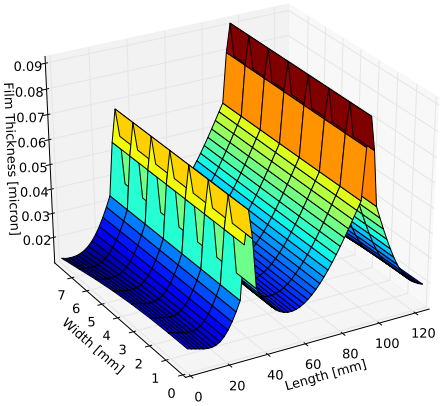

FIGURE 4.47: Crank angle $\theta = 0$

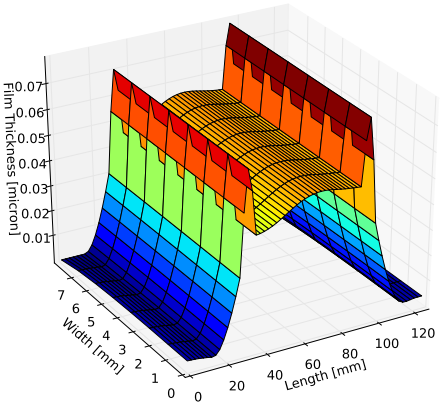

FIGURE 4.48: Crank angle $\theta = 180$

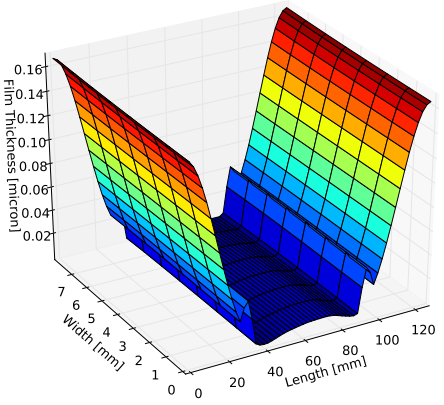

FIGURE 4.49: Crank angle $\theta = 360$

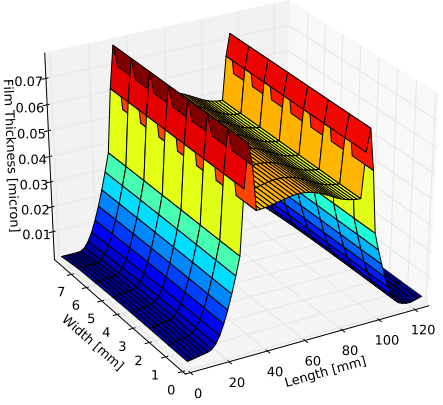

FIGURE 4.50: Crank angle $\theta = 540$

FIGURE 4.51: Film thickness distribution at different crank angle

Chapter 5

Further Applications of the Concept of Complementarity to Lubrication

In this thesis, the concept of complementarity has been applied to the analysis of lubrication problems in the presence of cavitation. Strozzi [36] proposed complementarity-oriented approach to the solution of other problem related to lubrication: the slip at the wall and the mixed lubrication.

The complementarity formulation of the Reynolds equation for EHL problem presented in this thesis has been developed in the case of a no-slip boundary and for a fully lubricated bearing (no dry contact is allowed), but it can be combined with the formulations proposed in [36] to consider the effect of the slip at the wall and to allow dry contact in case the hydrodynamic lubrication it is not sufficient to sustain the external load.

In the following, the slip at the wall (i) and the mixed lubrication (ii) problems will be discussed and the related complementarity formulation will be unfolded.

5.1 Slip at The Wall

"Now don't you forget this! Why I should stick my neck out for you is far beyond my capacity!"

C-3PO, Star Wars

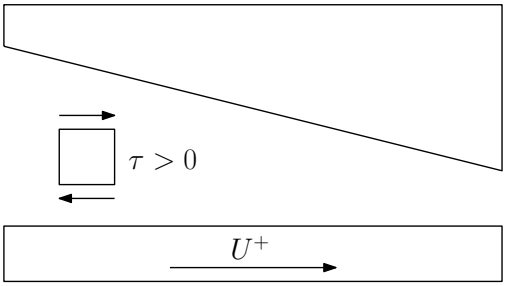

FIGURE 5.1: Meaning of symbols τ and U^+ and the the shear stress sign convention for the tangential velocity slip problem

In this section, the problem of the slip at the wall is tackled. Recently, many works [37–39] analysed the experimental evidence of the slippage of the fluid film with respect to the wetted surface.

it is possible to evaluate the shear stress that acts between the fluid layer and the solid surface, τ, that is due to the gradient of velocity in the thickness direction. See Fig.5.1 for sign convention. For Newtonian fluids:

$$\tau = \mu \frac{dU}{dz} \tag{5.1}$$

5.1.1 Complementarity Formulation for the Tangential Velocity Slip Problem

In the following, the work in [36] is reported and its integration to the proposed complementarity formulation for lubrication problems in the presence of cavitation is discussed.

The maximum value of shear stress that the surface tension force can provide is tau^+ and is called critical shear stress. When the value of tau is greater than the critical shear stress, tau^+, the fluid layer at direct contact with the solid surface slips at a relative speed different than zero.

Now two variables are defined:

$$\Delta\tau = \tau - \tau^+ \tag{5.2}$$

$$\Delta U = U^+ - U \tag{5.3}$$

where τ^+ is the critical shear stress, tau is the shear stress, U^+ is the sliding velocity of the solid surface and U the tangential velocity of the fluid layer.

With the simple model of slip presented, the two variables $\Delta\tau$ and ΔU are complementarity. The demonstration is straightforward: when the shear stress is lower than the

critical value, $\Delta\tau > 0$ and the fluid layer does not slip, so $\Delta U = 0$. When the shear stress reach the critical value, instead, $\tau = \tau^+$ and, thus, $\Delta\tau = 0$ because the stress is limited and can not exceed the critical value. The fluid layer slip and there is relative motion between fluid and solid, so $U < U^+$ and $\Delta U > 0$.

It is also possible that $U > U^+$: in this case a different definition of ΔU should be employed. It is possible to handle simultaneously slippage where $U > U^+$ in certain zones of the domain and $U < U^+$ in others. The formulation become more complex and is outside the scope of this work. The detailed discussion of the problem of the tangential velocity slip will be the topic of future contribution.

The Reynolds equation for one quasi-stationary, unidimensional, isothermal, isoviscous and hydrodynamic problems is:

$$\frac{d}{dx}\left(\frac{h^3}{\mu}\frac{dp}{dx} - 6Uh\right) = 0. \tag{5.4}$$

At the boundaries the pressure is fixed:

$$\begin{aligned} p(0) &= p_i \\ p(a) &= p_a. \end{aligned} \tag{5.5}$$

By integrating twice Eqn.(5.4) and by imposing the boundary conditions of Eqn.(5.5), the expression of the fluid pressure, p, as a function of U is derived:

$$p(x) = 6\mu\int_0^x \frac{U}{h^2}dy + \left[(p_a - p_i) - 6\mu\int_0^a \frac{U}{h^2}dy\right]\frac{\int_0^x \frac{1}{h^3}dy}{\int_0^a \frac{1}{h^3}dy} + p_i. \tag{5.6}$$

The manipulation above aims at expressing the fluid shear stress, τ, at the fluid layer contacting the sliding profile, as a function of the velocity, U, of the fluid layer in contact with the sliding surface.

The shear stress within the fluid in contact with the sliding profile (for z=0) is:

$$\tau|_{z=0} = \frac{h}{2}\frac{dp}{dx} + U\frac{\mu}{h}. \tag{5.7}$$

By substituting Eqn.(5.6) into Eqn.(5.7) one obtains:

$$\tau|_{z=0} = 4\mu\frac{U}{h} - 3\frac{\mu}{h^2}\frac{\int_0^a \frac{U}{h^2}dy}{\int_0^a \frac{1}{h^3}dy} + \frac{(p_a - p_i)}{2h^2\int_0^a \frac{1}{h^3}dy}. \tag{5.8}$$

This functional expression can be given a compact form:

$$\tau = LU + Q. \tag{5.9}$$

where L and Q are identified by comparing Eqn.(5.8) with Eqn.(5.9).

By adding and subtracting τ^+ and U^+ to both the side of Eqn.(5.9) it is possible to recast the equation in terms of the two complementary variables.

$$\tau - \tau^+ = L(U^+ - U) + Q - \tau^+ - LU^+. \tag{5.10}$$

In terms of $\Delta\tau$ and ΔU:

$$\Delta\tau = L\Delta U + Q - \tau^+ - LU^+. \tag{5.11}$$

The linear complementarity formulation for lubrication problems where tangential slippage occurs can be stated as: find $\Delta\tau$ and ΔU such that

$$\begin{aligned} &\Delta\tau = L\Delta U + Q - \tau^+ - LU^+ \\ &\Delta\tau > 0 \\ &\Delta U > 0 \\ &\Delta\tau\Delta U = 0. \end{aligned} \tag{5.12}$$

The numerical implementation in trivial and is left as an exercise to the interested reader.

5.1.2 Complementarity Formulation For the Slip at the Wall Problem in the Presence of Cavitation

It is possible to couple the linear complementarity system of Eqn.(2.26) with the formulation for the tangential velocity slip problem discussed above.

The simultaneous solution of Eqn.(2.26) and Eqn.(5.11) can be achieved with two iterative step:

1. Solution of the Reynolds equation in terms of p and r
2. Detection of slippage and evaluation of the velocity of the fluid layer

In particular Eqn.(2.26) solves for p and r the lubrication problem given the sliding velocity, U. The pressure p is used in Eqn.(5.11) to detect if slip occurs and to evaluate

the local velocity of the fluid layer, U. The new velocity distribution is then used to solve again Eqn. (2.26) iteratively until convergence.

It is possible to write a linear complementarity formulation that solves simultaneously the system of equations of Eqn. (2.26) and the system that describes the slip at the wall of Eqn.(5.12).

A fully coupled method that solves simultaneously the EHL Reynolds equation and Eqn.(5.11) can be developed. It will be the topic of future development.

5.2 Mixed Lubrication

Usually, the lubrication behaviour is classified in three different regimes:

- Fluid film lubrication
- Mixed lubrication
- Boundary lubrication

The fluid film lubrication regime occurs when two solid surfaces are in relative motion relative to one another and the load is fully supported by the lubricant film within them. The solid-solid contact is avoided and the solid races are fully wetted.

As the load capacity of the fluid film decreases, it is possible that contact between the solid surfaces asperities occurs. In this case the load is sustained partly by the hydrodynamic lubrication and partly by the asperities dry contact. This regime is called mixed lubrication regime.

If the load capacity of the fluid is low enough to allow close contact of the bodies and the dry contact assume a relevant part on the load bearing, the regime is called boundary lubrication regime.

5.2.1 Complementarity Formulation for Dry Contact Problems

The complementarity formulation for dry contact is well established and links the contact pressure to the gap between the surfaces as follow:

$$Cp_d + h_d = g \tag{5.13}$$

where C is the compliance matrix reduced to the boundary nodes of the contact bodies, p_d is the dry contact pressure, h_d is the distance of two corresponding points and g is the initial gap.

The inversion of C gives the stiffness matrix, K. Eqn. (5.13) can be recasted in terms of the pressure, p:

$$p_d + Kh_d = Kg. \tag{5.14}$$

Pressure p_d and point distance h_d are complementary variables. Where the distance h_d is greater than zero no contact occurs, thus $p = 0$. On the other hand, when the distance h_d equals zero, then the contact pressure $p \geq 0$.

The linear complementary problem of the dry contact is then defined as follows. Find p_d and h_d such that:

$$\begin{aligned} &p_d + Kh_d = Kg \\ &p_d > 0 \\ &h_d > 0 \\ &p_d h_d \neq 0. \end{aligned} \tag{5.15}$$

A suitable solver for LCP problem can be employed to solve the problem in p_d and h_d.

5.2.2 EHL Formulation for Mixed Lubrication in the Presence of Cavitation

The formulation briefly unrolled above can be applied to the EHL complementarity formulation in the presence of cavitation of Chapter 3 to solve mixed lubrication problems.

First, the equation to evaluate the total film thickness, Eqn. (3.1), is extended to consider dry contact:

$$h = h_g + h_e + h_d \tag{5.16}$$

where h_d is the amount of thickness due to the dry contact and the other symbols maintain the meaning explained in Sec.3.1. The terms h_e and h_d both are evaluated by multiplication of the compliance matrix C with the corresponding pressure (namely, lubricant pressure and dry contact pressure).

The correct detection of dry contact in an EHL lubricated bearing can be achieved in two steps:

1. The complementarity EHL Reynolds equation is solved

2. The complementarity dry contact system is solved

The solution of the EHL Reynolds equation provides the initial gap that is used to solve the dry contact. In fact, when the fluid film pressure is evaluated, it is possible to calculate the total film thickness with Eqn.(3.1). h, in the case of very high load or low sliding speed and viscosity, may become negative in some points of the domain. In this case, the second step is performed: the total film thickness h is used as initial gap ($g = h$) and the system of linear equation of Eqn. is solved. The resulting pressure vector, p_d, will present non-null values where dry contact occurs. The corresponding values of fluid pressure, p, are reset to zero.

The total film thickness, h, then becomes:

$$h = h_g + Cp + Cp_d \tag{5.17}$$

The fluid and dry pressure vectors can be merged together because the compliance matrix C this the same in both cases. The dry contact pressure, p_d, elements with values greater than zero replace the corresponding fluid pressure, p, elements. The merged pressure vector, p_m, can be adopted to lead back Eqn.(5.17) to Eqn. (3.1).

$$h = h_g + Cp_m \tag{5.18}$$

This modification to the film thickness due to dry contact requires to iterate the procedure to ensure the correctness of the solution.

A fully coupled method, that solves simultaneously the EHL Reynolds equation and Eqn.(5.14) in every nodes of the domain can be developed. It is a work in progress and will be the topic of future contribution.

Chapter 6

Conclusions and Future Development

6.1 Conclusions

In this work, a EHL Reynolds based model was developed to deal with lubrication problems in the presence of cavitation for compressible, piezoviscous and non Newtonian fluids.

First, the one-dimensional mass-conserving complementarity formulation derived by Giacopini et al. [10] has been extended to two-dimensional domains, and it has been modified to include fluid compressibility, piezoviscosity and non-Newtonian behaviour.

Then, the elastic deflection has been taken into account and a suitable and fast formulation to solve EHL problems inspired by the works in [31] and [32] has been derived.

The Finite Element algorithm developed to solve the resulting LCP has been tested and successfully validated by comparison with existing alternative algorithms and full CFD simulations. The test cases presented have demonstrated that the numerical approach proposed is robust and versatile. The methodology developed allows the employment of a wide range of different models for the formulation of compressibility, piezoviscosity, shear-thinning of the lubricant and elastic deflection.

6.2 Future Development

This work lays the foundations for the analysis of a wide range of different application.

One proposal is to apply the proposed formulation to the analysis of lubrication performance of textured and rough surfaces, which is a field of actual interest.

Regarding the engine components analysis, this formulation has been applied to the connecting rod big end lubrication analysis. Similar applications that can be analysed with the algorithm developed are the crankshaft bearings and the connecting rod small end. Moreover, the camshaft bearings and the cam-follower contact can be studied with the implementation proposed.

Others interesting applications are the piston-skirt and the piston ring lubrication analysis. The need of reduce the fuel consumption and improve the efficiency of the internal combustion engine led many research towards the optimization of such lubrication contacts, and the formulation and algorithm proposed is indicated for this aim.

As Chapter 5 proposes, the coupling of the complementarity formulation for EHL lubrication problems in the presence of cavitation with the complementarity formulations of the slip at the wall and of the mixed lubrication is a very interesting and innovative development. In fact, there are very few existing research on this topic and the proposed formulation showed high potentialities.

Appendix A

Analytical model for two dimensional pure squeeze motion

A.1 Analytical model for two dimensional pure squeeze motion

In this Appendix, the analytical model for a pure squeeze motion in a two dimensional axisymmetric domain is presented. This has been employed to validate the capabilities of the complementarity formulation proposed in this thesis. The following discussion is based on the analytical solution provided in [35]. Consider the equation governing the problem being the Reynolds equation recasted in polar coordinates that, for this particular axisymmetric case, does not depend on the angular coordinate θ:

$$\frac{\partial}{\partial r}\left(rh^3\frac{\partial p}{\partial r}\right) - 12\mu r\frac{\partial h}{\partial t} = 0. \tag{A.1}$$

According to [35], three periods are considered during oscillations:

(i) *Cavitation not yet appearing.* The pressure distribution is calculated using Eqn.(A.8). Being r_a the radius of the plates, the boundary condition $p(r,0) = p_0$ and $p(r_a,t) = p_0$ are employed and the pressure evolution at the center of the plates $p(0,t)$ is evaluated as a function of t. When, during the plates separation, the calculated pressure at the plate center becomes less or equal than the cavitation pressure, p_{cav}, cavitation occurs. The time t_{sc} when cavitation starts is stored.

(ii) *Cavitation area is evolving.* During the expansion of the cavitation region the quantity of liquid found at the cavitation boundary is deposed on the solid surfaces and later it will participate to the reformation process. Numerically, the film thickness at

the cavitation boundary is memorized, in order to determinate the liquid rate later. In particular, the liquid rate in the cavitated area is defined as:

$$\Theta(r,t) = \frac{h(r,t_0)}{h(r,t)} \tag{A.2}$$

and t_{rs} is defined as the time when the cavitation occurs at the r position i.e., the time when the pressure becomes equal to p_{cav} at the r location. For a rupture boundary, at the interface between cavitated and active region, r_c, the following boundary conditions are considered:

$$\begin{aligned} p &= p_{cav} \\ \frac{\partial p}{\partial r} &= 0 \ \text{ (Reynolds}'\text{s condition).} \end{aligned} \tag{A.3}$$

When the cavitation region stops its growth the reformation starts. The time t_{eg} when cavitation growth ends is stored.

(iii) *Cavitation area is reducing.* The full-film is reforming and the quantity of liquid left on the surfaces in (ii) participates to this reformation. The mass conserving condition at the reformation boundary is given by the flow balance equation. The flow rate in the active zone near the boundary is given in the squeeze case by the Poiseuille velocity profile across the film thickness:

$$Q\left(\Omega^{\pm}\right) = -\frac{h^3}{12\mu}\frac{\partial p}{\partial r}. \tag{A.4}$$

In the case of a reformation boundary, the balance of the flow on both sides of the interface full film/ cavitation zone gives the velocity of the reformation boundary:

$$\dot{r_c} = \frac{Q\left(\Omega^{\pm}\right)}{h(1-\theta)}, \tag{A.5}$$

When cavitation region vanishes the full-film occupies the whole domain.

Following the above scheme, to define the evolution of the cavitated area, a differential equation arises with the variable being the position of the cavitation boundary. Considering the motion law governing the relative position between the two circular plates being a sinusoidal function of time only (i.e. the two plates are plane and parallel):

$$h(t) = h_{min} + h_a\left(1 - cos(\omega t)\right). \tag{A.6}$$

Eqn. (A.1) can be rewritten as:

$$h(t)^3 \frac{\partial}{\partial r}\left(r\frac{\partial p}{\partial r}\right) - 12\mu r v(t) = 0, \tag{A.7}$$

where $v(t)$ is the squeeze speed, and it follows from derivation of Eqn. (A.6) with respect to time. Integrating Eqn. (A.1) twice, we obtain the analytical formula of the pressure:

$$p = \frac{3v(t)\mu r^2}{h(t)^2} + C1(r,t)ln(r) + C2(r,t). \tag{A.8}$$

For the cavitation growth, the differential equation defining the interface position is obtained by a temporal derivation of the Reynolds' condition of Eqn. (A.3) while, for the case of cavitation collapse, the equation that gives the boundary velocity comes from Eqn. (A.5), by evaluating $\partial p/\partial r$ at the position $r = r_c$.

Both the two differential equation described above are solved employing a fourth-order Runge-Kutta integration method.

Appendix B

Publications by the Author

B.1 Publications on the Topic

- L. Bertocchi, M. Giacopini, D. Dini. "Analysis of the Lubrication Regimes at the Small End and Big End of a Connecting Rod of a High Performance Motorbike Engine", ASME/STLE 2012 International Joint Tribology Conference, October 7-10, 2012, Denver, Colorado
- M.Giacopini, A. Strozzi, L. Bertocchi, M. T. Fowell, D. Dini. "Formulazione in termini di complementariet della cavitazione in contatti lubrificati", VI Giornata di studio Ettore Funaioli, 16 luglio 2012, Bologna.
- M. Giacopini, L. Bertocchi, M. T. Fowell, D. Dini and A. Strozzi. "A mass-conserving complementarity formulation to study textured bearings in the presence of cavitation for non-Newtonian and compressible fluids", International Joint Tribology Conference, October 24-26, Los Angeles, 2011

Currently under review

- L. Bertocchi, D. Dini, M. Giacopini, M. T. Fowell, A. Baldini. "Fluid film lubrication in the presence of cavitation: a mass-conserving two-dimensional formulation for compressible, piezoviscous and non-newtonian fluids"

B.2 Other Publications

- A. Strozzi, A., Baldini, M. Giacopini, E. Bertocchi and L. Bertocchi. "Achievement of a uniform contact pressure in a shafthub press-fit", Proceedings of the Institution of Mechanical Engineers, Part C: Journal of Mechanical Engineering Science, 2012

- A. Strozzi, A. Baldini, M. Giacopini, E. Bertocchi and L. Bertocchi. "Maximum equivalent stress in a pin-loaded lug in the presence of initial clearance", J. Strain Analysis, 2011, 46(8), pp 760-771

- A. Strozzi, A. Baldini, M. Giacopini, E. Bertocchi and L. Bertocchi. "Normalization of the stress concentrations at the rounded edges of a shaft-hub interference fit", J. Strain Analysis, 2011, 46(6), pp 478-491

- A. Strozzi, M. Giacopini, A. Baldini, E. Bertocchi, L. Bertocchi. "Stress concentrations at the rounded edges of a shaft-hub interference fit expressed in terms of a coefficient normalizing the coupling geometry and the Young's modulus effects", ASME 2012 International Mechanical Engineering Congress and Exposition, November 9-15, 2012, Houston, Texas

- A. Strozzi, A. Baldini, M. Giacopini, E. Bertocchi, L. Bertocchi, E. Campioni, S. Mantovani, O. Quareshi "Torque Transmission by Friction in a Keyed Shaft-Hub Press-Fits", 9th International Conference On Advanced Manufacturing Systems And Technology, Mali Losinj, Croatia, June 16-17, 2011

- A. Strozzi, L. Bertocchi, E. Campioni. "Normalization of the stress concentrations at the interference fit between a cylindrical shaft and a hub with rounded edges", Atti dell aQuarta giornata di studio Ettore Funaioli, Astrisco Edizioni, pp.231-240, 2011

- A. Strozzi, A. Baldini, M. Giacopini, E. Bertocchi, L. Bertocchi, S. Mantovani, R. Rosi"Normalization of the stress concentrations at the interference fit between a cylindrical shaft and a hub with rounded edges", 37th Solid Mechanics Conference, Warsaw, Poland, September 610, 2010

- L. Bertocchi, A. Libbra e A. Muscio. "Microgeneratori ad effetto Peltier per dispositivi di contabilizzazione termica". XXVI Congresso Nazionale UIT sulla Trasmissione del Calore, 23-25 Giugno 2008, Palermo

Bibliography

[1] Roberto Ausas, Patrick Ragot, Jorge Leiva, Mohammed Jai, Guy Bayada, and Gustavo C. Buscaglia. The impact of the cavitation model in the analysis of micro-textured lubricated journal bearings. *Journal of Tribology*, 129(4):868–875, 2007.

[2] B. Jakobsson and L. Floberg. The finite journal bearing considering vaporization,. *Transactions of Chalmers University of Technology*, page 190, 1957.

[3] H. G. Elrod and M. L. Adams. A computer program for cavitation and starvation problems. *Proceeding of the First Leeds-Lyon Symposium on Tribology - Cavitation and Related Phenomena in Lubrication, D. Dowson, M. Godet and C. M. Taylor*, pages 37–41, 1974.

[4] H. G. Elrod. A cavitation algorithm. *Journal of Lubrication Technology*, 103(3): 350–354, 1981.

[5] D. Vijayaraghavan and T.G. Keith. Development and evaluation of a cavitation algorithm. *Tribology Transactions*, 32(2):225–233, 1989.

[6] Fredrik Sahlin, Andreas Almqvist, Roland Larsson, and Sergei Glavatskih. A cavitation algorithm for arbitrary lubricant compressibility. *Tribology International*, 40 (8):1294 – 1300, 2007. ISSN 0301-679X.

[7] M. Kostreva. Elasto-hydrodynamic lubrication: A non-linear complementarity problem. *Int. J. Numer. Methods Fluids*, 4(4):377–397, 1984.

[8] Kong Ping Oh. The numerical solution of dynamically loaded elastohydrodynamic contact as a nonlinear complementarity problem. *Journal of Tribology*, 106(1):88–95, 1984.

[9] K. P. Oh and P. K. Goenka. The elastohydrodynamic solution of journal bearings under dynamic loading. *Journal of Tribology*, 107(3):389–394, 1985.

[10] Matteo Giacopini, Mark T. Fowell, Daniele Dini, and Antonio Strozzi. A mass-conserving complementarity formulation to study lubricant films in the presence of cavitation. *Journal of Tribology*, 132(4):041702, 2010.

[11] A. Almqvist, E.K. Essel, L.-E. Persson, and Peter Wall. Homogenization of the unstationary incompressible reynolds equation. *Tribology International*, 40(9):1344 – 1350, 2007. ISSN 0301-679X.

[12] A. V. Olver, M. T. Fowell, H. A. Spikes, and I. G. Pegg. inlet suction, a load support mechanism in non-convergent, pocketed, hydrodynamic bearings. *Proceedings of the Institution of Mechanical Engineers, Part J: Journal of Engineering Tribology*, 220 (2):105–108, 2006.

[13] M. Fowell, AV Olver, AD Gosman, HA Spikes, and I. Pegg. Entrainment and inlet suction: two mechanisms of hydrodynamic lubrication in textured bearings. *Journal of tribology*, 129:336, 2007.

[14] Roberto F. Ausas, Mohammed Jai, and Gustavo C. Buscaglia. A mass-conserving algorithm for dynamical lubrication problems with cavitation. *Journal of Tribology*, 131, 2009.

[15] Torbjorn Almqvist Fredrik Sahlin, Sergei B. Glavatskih and Roland Larsson. Two-dimensional cfd-analysis of micro-patterned surfaces in hydrodynamic lubrication. *Journal of Tribology*, 127(1):96–102, 2005.

[16] Stathis Ioannides Markus Hartinger, David Gosman and Hugh A. Spikes. Cfd modelling of elastohydrodynamic lubrication. *ASME Conference Proceedings*, 2005 (4):531*532, 2005.

[17] D. Dowson and GR. Higginson. *Elastodydro-dynamic Lubrication*. Pergamon Press, Oxford, 1966.

[18] Jonas Sthl and Bo O. Jacobson. Compressibility of lubricants at high pressures. *Tribology Transactions*, 46(4):592–599, 2003.

[19] Roger Tuomas and Ove Isaksson. Compressibility of oil/refrigerant lubricants in elasto-hydrodynamic contacts. *Journal of Tribology*, 128(1):218–220, 2006.

[20] Bo O. Jacobson and Pascal Vinet. A model for the influence of pressure on the bulk modulus and the influence of temperature on the solidification pressure for liquid lubricants. *Journal of Tribology*, 109(4):709–714, 1987.

[21] C.H. Venner and J. Bos. Effects of lubricant compressibility on the film thickness in ehl line and circular contacts. *Wear*, 173(12):151 – 165, 1994. ISSN 0043-1648.

[22] C.J.A Roelands. *Correlational aspects of the viscosity-temperature-pressure relationship of lubricating oils*. PhD thesis, TU Delft, Delft University of Technology, April 1966.

[23] Arthur K. Doolittle. Studies in newtonian flow. ii. the dependence of the viscosity of liquids on free-space. *Journal of Applied Physics*, 22(12):1471 –1475, dec 1951. ISSN 0021-8979.

[24] D. Rh. Gwynllyw, A. R. Davies, and T. N. Phillips. On the effects of a piezoviscous lubricant on the dynamics of a journal bearing. *Journal of Rheology*, 40(6):1239–1266, 1996.

[25] R.S.A. Grieve and Hugh A. Spikes. Temperature and shear stress in thin film ehd contacts. In *Thinning Films and Tribological Interfaces Proceedings of the 26th Leeds-Lyon Symposium on Tribology*, volume 38 of *Tribology Series*, pages 511 – 522. Elsevier, 2000.

[26] O.C. Zienkiewicz and Freng Emeritus. *The Finite Element Method Fifth edition Volume 3: Fluid Dynamics*. Butterworth-Heinemann, 2000.

[27] R. H. Gallagher. Fundamentals of the finite element method, hartley grandin, jr., macmillan publishing co., n.y., 1986. no. of pages: 528. isbn 0-02-345480-6. *International Journal for Numerical Methods in Engineering*, 23(11):2169–2169, 1986. ISSN 1097-0207. doi: 10.1002/nme.1620231114.

[28] Guy Payre, Michel De Broissia, and Jacques Bazinet. An upwind finite element method via numerical intergration. *International Journal for Numerical Methods in Engineering*, 18(3):381–396, 1982. ISSN 1097-0207. doi: 10.1002/nme.1620180306. URL http://dx.doi.org/10.1002/nme.1620180306.

[29] K. L. Johnson. *Contact Mechanics*. Cambridge University Press, Cambridge, U.K., 1985.

[30] R. Gohar. *Elastohydrodynamics*. Imperial College Press, London, U.K., 2001.

[31] S. M. Rohde and K. P. Oh. A unified treatment of thick and thin film elastohydrodynamic problems by using higher order element methods. *Proceedings of the Royal Society of London. A. Mathematical and Physical Sciences*, 343(1634):315–331, 1975. doi: 10.1098/rspa.1975.0068. URL http://rspa.royalsocietypublishing.org/content/343/1634/315.abstract.

[32] L. E. C. Ruskell. A rapidly converging theoretical solution of the elastohydrodynamic problem for rectangular rubber seals. *Journal of Mechanical Engineering Science*, 22(1):9–16, 1980. URL http://jms.sagepub.com/content/22/1/9.abstract.

[33] Marcus Hartinger. *CFD Modelling of Elastohydrodynamic Lubrication*. PhD thesis, Imperial College London, November 2007.

[34] M. Hartinger, M.L. Dumont, S. Ioannides, D. Gosman, and H. Spikes. Cfd modeling of a thermal and shear-thinning elastohydrodynamic line contact. *Journal of Tribology*, 130, 2008.

[35] Virgil Optasanu and Dominique Bonneau. Finite element mass-conserving cavitation algorithm in pure squeeze motion. validation/application to a connecting-rod small end bearing. *Journal of Tribology*, 122(1):162–169, 2000.

[36] Antonio Strozzi. Formulation of three lubrication problems in terms of complementarity. *Wear*, 104(2):103 – 119, 1985. ISSN 0043-1648. doi: 10.1016/0043-1648(85)90056-0. URL http://www.sciencedirect.com/science/article/pii/0043164885900560.

[37] HA Spikes. Slip at the wall: evidence and tribological implications. In G. Dalmaz D. Dowson, M. Priest and A.A Lubrecht, editors, *Tribological Research and Design for Engineering Systems Proceedings of the 29th Leeds-Lyon Symposium on Tribology*, volume 41 of *Tribology Series*, pages 525 – 535. Elsevier, 2003. doi: 10.1016/S0167-8922(03)80167-0. URL http://www.sciencedirect.com/science/article/pii/S0167892203801670.

[38] HA Spikes. The half-wetted bearing. part 1: extended reynolds equation. *Proceedings of the Institution of Mechanical Engineers: Journal of engineering tribology*, 217:1, 2003.

[39] HA Spikes. The half-wetted bearing. part 2: potential application in low load contacts. *Proceedings of the Institution of Mechanical Engineers: Journal of engineering tribology*, 217:15, 2003.